

Intra- and Interobserver agreement
in assessment of macular diseases
using high-definition spectral-
domain optical coherence
tomography

Inaugural-Dissertation
zur Erlangung des Doktorgrades
der Medizin

der Medizinischen Fakultät
der Eberhard Karls Universität
zu Tübingen

vorgelegt von

Treviño Rodríguez, Hugo
Alejandro

2016

Dekan: Professor Dr. B. Autenrieth

Berichterstatter: Professor Dr. F. Gelisken

Berichterstatter: Privatdozent Dr. M. Lüke

To my parents:

Who gave me a wonderful life, and all the support and opportunities.

To my wife, Krystal:

Who has taught me how to be a better human being, who has beared with me for so many years, and has shared the good and the bad.

To my children, Julia and Aidan:

Who have taught me how much my parents love me, and for all the happiness they have brought us.

Contents

Abbreviations

1. Introduction	1
1.1 Overview of the Macula	3
1.2 Retinal structures	5
1.3 History of Optical Coherence Tomography (OCT)	7
1.4 Principles of OCT	9
1.5 Time-domain OCT (TD-OCT)	10
1.6 Limitations of TD-OCT	13
1.7 Spectral/Fourier-domain OCT (SD-OCT)	14
1.8 Limitations of SD-OCT	15
1.9 Advantages of SD-OCT	15
1.10 Spectralis OCT	17
1.11 OCT characteristics in Macula	18
1.12 OCT findings in Macular Diseases	20
1.13 Pattern of OCT in Retinal Vascular Diseases	22
1.13.1 OCT in Diabetic Macular Edema (DME)	22
1.13.2 OCT in Branch Retinal Vein Occlusion (BRVO)	25
1.13.3 OCT in Central Retinal Vein Occlusion (CRVO)	27
1.13.4 Principles of the treatment of Retinal Vascular Diseases	28

1.14	OCT in Vitreoretinal Interface Disorders	29
1.14.1	Vitreomacular Traction Syndrome (VMTS)	29
1.14.2	Epiretinal Membrane (ERM)	31
1.14.3	OCT in Macular Holes	33
1.15	OCT in Age-Related Macular Degeneration (ARMD)	37
1.15.1	Non-neovascular ARMD	38
1.15.2	Neovascular ARMD	42
1.15.3	Treatment of ARMD	45
1.16	Anti-VEGF treatments	46
1.16.1	Ranibizumab (Lucentis)	47
1.16.2	Bevacizumab (Avastin)	48
1.16.3	Pegaptanib (Macugen)	49
1.16.4	Aflibercept (Eylea)	49
2.	Material and Methods	50
2.1	General objective	50
2.2	Hypothesis	50
2.3	Definitions	51
2.4	Study population	51
2.5	Inclusion criteria	52
2.6	Exclusion criteria	53
2.7	Selection of the study population	53
2.8	Design	54
2.9	Design description	54
2.10	Sample size	55
2.10.1	Analysis of the OCT scans	56
2.11	Evaluation method	56

2.11.1	Ophthalmologic examination	56
2.12	Examination protocol of the OCT	57
2.12.1	Preparation of the patient	57
2.12.2	Preparation of the OCT	57
2.12.3	Settings of Spectralis OCT	58
2.13	Artifacts and Gradability of the images	61
2.14	Color fundus photography, Fluorescein angiography and Indocyanine green angiography	61
2.15	Data analysis	62
2.16	Variables	66
2.17	Statistical analysis	68
2.18	Description of activities	69
3.	Results	70
3.1	Demographic data	70
3.2	Results of CRT in macular diseases	72
3.3	Intraobserver agreement in macular diseases (HT1-HT2)	72
3.4	Interobserver agreement in macular diseases: first analysis (HT1-ML3)	73
3.5	Interobserver agreement in macular diseases: second analysis (HT2-ML3)	74
3.6	Results of morphological findings (variables)	79

3.7	Total results of morphological findings	85
3.8	Results of nongradable morphological findings	87
4.	Discussion	89
5.	Summary	98
6.	Bibliography	102
7.	Deutsche Zusammenfassung	130
8.	Acknowledgements	134
9.	Curriculum vitae	137

List of Charts	Page
1. Central retinal thickness between intraobserver in macular diseases	76
2. Central retinal thickness between interobserver in macular diseases: first analysis	77
3. Central retinal thickness between interobserver in macular diseases: second analysis	78

List of Tables

1. Demographics data of patients with macular diseases	70
2. Gradability of OCT- images by observers in macular diseases	71
3. Intraobserver agreement in macular diseases	73
4. Interobserver agreement in macular diseases: first analysis	74
5. Interobserver agreement in macular diseases: second analysis	75
6. Result of Foveal depression (Fo_De)	79
7. Result of Epiretinal membrane (ERM)	80

8. Result of Vitreofoveal traction (VFT)	80
9. Result of Pseudocyst	80
10. Result of Splitting	81
11. Result of Verticalisation	81
12. Result of Macular hole (MH)	82
13. Result of Pseudomacular hole (PSM)	82
14. Result of Lamellar macular hole (LMH)	82
15. Result of Neurosensory detachment (NSD)	83
16. Result of Pigment epithelium detachment (PED)	83
17. Result of External limiting membrane (ELM)	84
18. Result of Photoreceptors inner and outer segments (IS/OS)	84
19. Degree of agreement in morphological findings	86
20. Nongradable morphological findings	88

Abbreviations

ARMD	Age-related macular degeneration
A-SCAN	Axial scan
BRVO	Branch retinal vein occlusion
CC	Coefficient correlation
CI	Confidence interval
CNV	Choroidal neovascularization
CME	Cystic macular edema
CRVO	Central retinal vein occlusion
CRT	Central retinal thickness
DM	Diabetes mellitus
DME	Diabetic macular edema
DR	Diabetic retinopathy
ELM	External limiting membrane
ERM	Epiretinal membrane
ETDRS	Early treatment of diabetic retinopathy study

FAZ	Foveal avascular zone
FIG	Figure
GA	Geographic atrophy
GCL	Ganglion cell layer
INL	Inner nuclear layer
ILM	Internal limiting membrane
IMH	Idiopathic macular hole
IPL	Inner plexiform layer
IS/OS	Inner and outer segment junction
LMH	Lamellar macular hole
MD	Mean difference
ME	Macular edema
MH	Macular hole
NSD	Neurosensory detachment of the retina
OCT	Optical coherence tomography
ONL	Outer nuclear layer
OPL	Outer plexiform layer
PED	Pigment epithelial detachment

PDR	Proliferative diabetic retinopathy
PDT	Photodynamic therapy
PSM	Pseudomacular hole
PVD	Posterior vitreous detachment
RNFL	Retinal nerve fiber layer
RPE	Retinal pigment epithelium
SD-OCT	Spectral domain optical coherence tomography
TD-OCT	Time domain optical coherence tomography
VEGF	Vascular endothelial growth factor
VFT	Vitreofoveal traction
VMTS	Vitreomacular traction syndrome

1. Introduction

The macula is a round highly pigmented yellow spot at the center of the posterior pole, it specialized for high acuity vision and it is important for reading, writing, driving, working on the computer and for trips (American Academy of ophthalmology, 2011).

Macular edema (ME) is the most common pathology of the macula, which is the main cause of impairment of central vision. Diseases such as diabetic macular edema (DME), age-related macular degeneration (ARMD) retinal vascular occlusive diseases, and vitreoretinal interface disorders are the most frequent reasons of ME. For more than 30 years, physicians have been trying to identify the macular edema in its initial state and to define their different etiologies (Nussenblat RB et al., 1987).

Since 2004, the clinical diagnosis of macular diseases and its treatment have been greatly improved due to remarkable advances of modern imaging technologies, such as Spectralis optical coherence tomography (OCT) that has a valuable technique for the detection, evaluation and monitoring the central retinal thickness measurement (CRT) in macular diseases (Wotjkowski M, Srinivasan et al., 2005; Alam S, Zawadzki RJ, Choi S, et al., 2006).

One of the most important innovations in the field of macular diseases has been the introduction of intravitreal drug delivery approaches for the treatment of posterior segment pathologies. These emerging modalities restore the permeability of the blood-retinal barrier by delivering drug compounds intravitreally with anti-inflammatory or anti-vascular endothelial growth factor drugs (Anti-VEGF).

Even though the morphological findings of the macular pathologies are known, the interpretation and measurements of them by OCT may vary. Some of these factors are; the quality of the captured images, the type of the OCT machine, the experience of the physician and at lastly the complexity of the findings.

The purpose of this study is to determine the degree of agreement between a general ophthalmologist and a retina specialist in the diagnosis and classification of the CRT and morphological findings found by Spectralis OCT in macular diseases. The reliability between the observers and intraobserver will be analyzed by statistical methods.

1.1 Overview of the Macula

The macula also called (macula lutea) is a round highly pigmented yellow spot at the posterior pole, lying inside the temporal vascular arcades; it has a diameter around 5 and 6mm, and subserves the central 15–20° of the visual field. This area contains a retinal pigment xanthophyll that confers hypofluorescence on angiography.

The macular area is centered on the fovea, a small concave depression retinal about 1.5 mm in diameter where the photoreceptor layer is formed exclusively by cones which constitute 10% of the retinal cones. The foveal cones are specialized and have an especially high density.

In the center of the fovea, there is the foveola, which is an avascular zone irrigated by the choriocapillaris. This part of the fovea does not contain inner nuclear layer and ganglion cell layer. The parafoveal area is a ring that is located 0.5 mm around the fovea. It is a region where the retina is thicker. The perifoveal area is a ring of 1.5 mm in diameter around the parafovea.

In the fovea there are 35,000 cones connecting with ganglion cells, so which is the area with the greatest capacity for visual discrimination of the retina (American Academy of ophthalmology, 2011) **(Fig. 1)**.

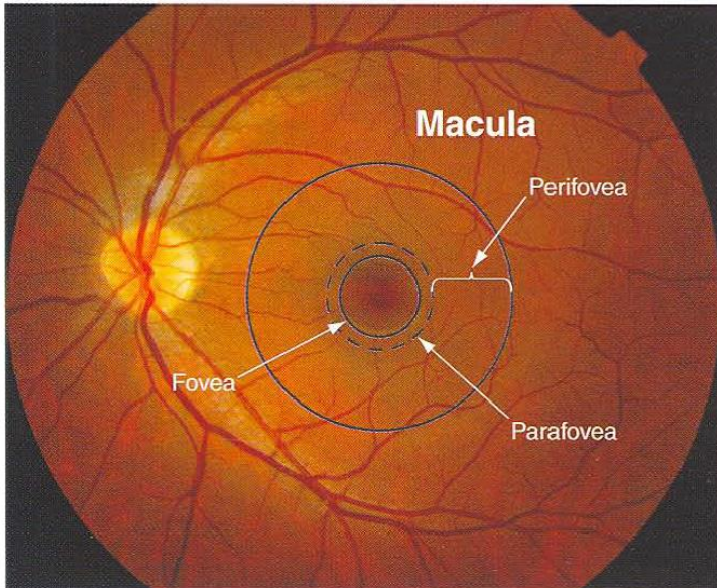


Fig. 1: Color photograph of the posterior pole. The anatomical fovea and foveola are in the center of the anatomical macula (by Spaide R.F. 2011).

1.2 Retinal Structures

The retina is composed of ten distinct layers. These layers are dark nuclear layers, containing cell bodies, or light plexiform layers, containing axons and dendrites (**Fig. 2**).

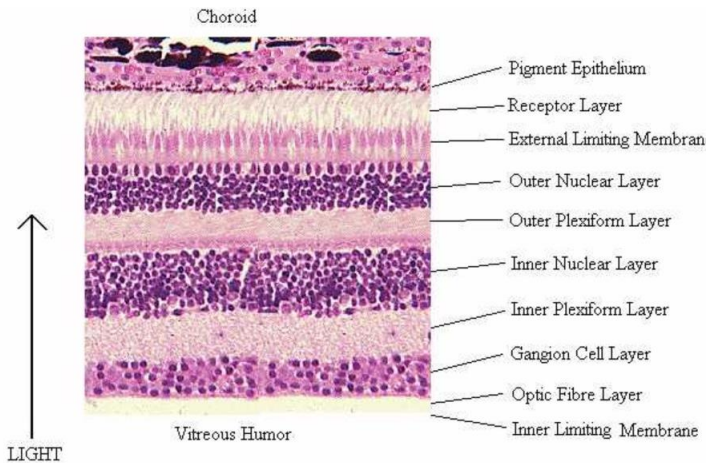


Fig. 2: Histological representation of the layers of the retina (by University of Bristol, Department of Anatomy 2000).

The retina is a highly organized structure with common-path neuronal axons of ganglion cells, which leads the visual information to the brain. It has an average of 4.6 million cones and 92 million rods (American Academy of ophthalmology, 2011).

The Internal limiting membrane (ILM) is the most superficial layer of the retina and is in contact with

the hyaloid of the vitreous gel. Histopathologically consists of the basement membrane of the extensions of the Müller cells. In the parafoveal and peripapillary region, the thickness of the ILM is about 2.5 microns. The side facing the vitreous cavity is thin, and the inside or retinal face is polished and irregular.

The ILM can act as a basis for cell growth and proliferation. Frequently involved in disorders that affect the vitreomacular interface, including epiretinal membranes (ERM), vitreomacular traction syndrome (VMTS) and macular hole (MH).

The inner third of the outer plexiform layer has a linear density where a synaptic connection between the photoreceptors and the processes of the bipolar cells occurs.

The retinal pigment epithelium (RPE) is composed of a single layer of hexagonally shape cuboidal cells, lying between Bruch's membrane and retina. These cells and the zonula occludentes constitute the outer blood retinal barrier, preventing extracellular fluid leaking into the subretinal space from the choriocapillaris, actively pump ions and water out of the subretinal space.

The central retinal artery and its branches, as well as the derivative venous return, are located in the inner retina, supplying nutrition to the inner nuclear layer. The nutritional value of the outer retina depends on the choriocapillaris, which is the innermost layer of the choroid that provides irrigation to the choroidal circulation.

The vitreous cavity has a capacity of about 3-4 ml, which is $\frac{4}{5}$ of the volume of the eyeball. The vitreous gel is tightly attached to the retina in the vitreous base, which extends to about 2-3 mm to the ora serrata.

The posterior hyaloid is strongly attached to the optic nerve, retinal vessels, macula and some retinal scars (Yanoff M, Duker JS, 2008; American Academy of ophthalmology, 2011).

1.3 History of Optical Coherence Tomography (OCT)

In 1991, OCT was described by Huang and associates, as a non-invasive medical diagnostic imaging, which performs micrometer resolution cross-sectional or tomographic imaging of the tissue using low coherence interferometry (Huang D, Swanson EA, Lin CP et al. 1991).

In 1993, the first in vivo OCT-images (displaying retinal structures) were published (Fercher AF., Hitzenberger CK, Drexler W et al., 1993; Hee MR, Swanson EA, Izatt J et al., 1993).

In 1995, time-domain optical coherence tomography (TD-OCT) was used for imaging macular diseases. Since then, OCT has become widely accepted for retinal thickness measurements and detection of the macular morphology in various retinal diseases (Puliafito CA, Hee MR, Lin CP et al., 1995).

In 2002, TD-OCT 300 (Stratus OCT) became available with an axial resolution of 10 μm and a scan velocity of 400 axial scans per second (Drexler W, Sattmann H et al., 2003).

Since 2004, higher-resolution spectral-domain OCT (SD-OCT) has entered clinical practice with reported resolutions of 1 to 5 μm as well as improved visualization of retinal morphologic and pathologic features. Today it is the current “gold standard” for posterior segment retinal tomography (Drexler W, Sattmann H et al., 2003; Wotjkowski M, Srinivasan et al., 2005; Alam S, Zawadzki RJ, Choi S et al., 2006).

1.4 Principles of OCT

OCT is analogous to B-mode ultrasound, except that uses light rather than wave sound. Unlike ultrasound, OCT does not require contact with the tissue examined. OCT is based on an apical measurement technique known as a low coherence interferometry, which can be used to measure ocular structures with high precision by measuring the light reflected from them (Huang D, Swanson EA, Lin CP et al., 1991).

In the OCT, a beam of light from a superluminescent diode is divided through a beam splitter into sample and reference beams (**Fig. 3**). Light from the sample beam is directed toward the tissue of interest. The light will be reflected with different echo time delays. Light from the reference beam is reflected from a different mirror located at a known distance. Both the reflected reference and sample beams are combined by a modified Michelson interferometer and detected by the OCT (Huang D, Swanson EA, Lin CP et al., 1991; Hee MR, Izatt JA, Swanson EA et al., 1995).

Detection of these beams is based on time-domain or spectral-domain protocols.

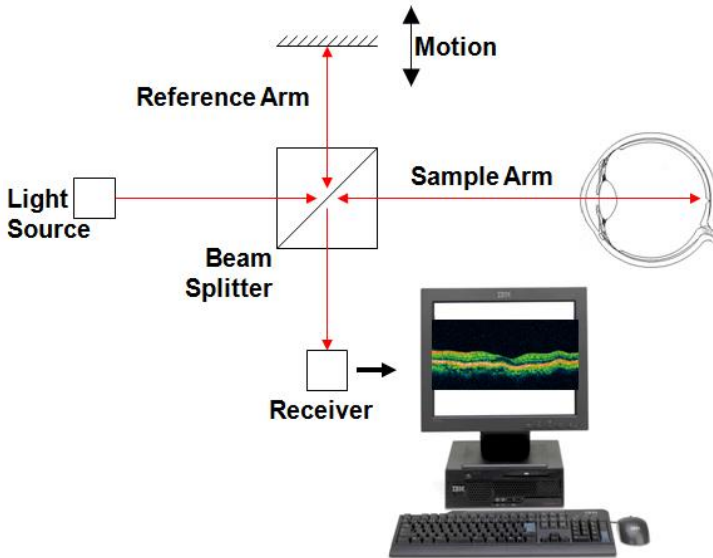


Fig.3: Principle of a Michelson interferometer type OCT system (by Jansz 2012).

1.5 Time-domain OCT (TD-OCT)

In TD-OCT, the position of the reference mirror is adjusted, creating different time delays for the echoes of the reference beam. Axial scans (A-scan) are obtained by directing the sample beam at different tissue depths and recording the reflected light echoes (Hee MR, Puliafito CA et al., 1995).

An example of TD-OCT is the Stratus-OCT, which has a resolution of $<10\ \mu\text{m}$ and can make from 128 to 768 A-scan in a single scan pass. Each A-scan has 1,024 data points and is 2mm long. By scanning the sample beam of light in a transverse direction, a cross sectional OCT (B-scan) image is obtained. Once the information has been obtained, a tomography is constructed using a false color scale that represents the amount of light backscattering from microstructures at different depths of the imaged tissue.

The images in TD-OCT are displayed in false color scale, bright colors such as red to white represent high reflectivity and dark colors such a blue to black represent minimal or no reflectivity (Hee MR, Puliafito CA et al., 1995) **(Fig. 4)**.

The ganglion cell layers (GCL), the inner nuclear layer (INL) and the outer nuclear layer (ONL) have a low reflectivity, and therefore appear blue-black in the false color scale. Conversely, the retinal pigment epithelium (RPE)/choriocapillaris and the retinal nerve fiber layer (RNFL), exhibit a high reflectivity (Toth CA, 1997).

The hyper-reflective band at the level of the RPE/choriocapillaris is actually composed of two highly reflective lines separated from each other by

one thin layer of low to moderate reflectivity. The inner highly reflective line corresponds to the junction of the photoreceptor's outer and inner segments (IS/OS). The outer highly reflective line corresponds to the RPE/choriocapillaris. Traditionally, the inner and outer retinal boundaries have been defined as the INL and RPE respectively (Costa RA et al., 2004; Pons ME et al., 2005; Sadda SR et al., 2007) (Fig. 4).

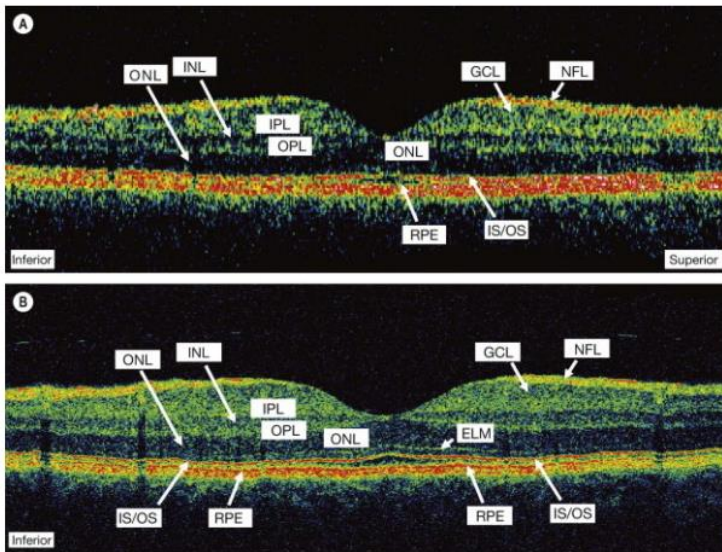


Fig. 4: The time-domain Stratus OCT, the images are displayed in false color. High reflectivity structures are depicted as red, intermediate as green-yellow and low reflectivity as blue-black. High resolution OCT (B) has the ability to identify fine retinal structures such as the external limiting membrane and ganglion cell layer which

are not visualized as clearly with standard resolution (A). NFL: Nerve fiber layer, GCL: Ganglion cell layer, IPL: Inner plexiform layer, INL: Inner nuclear layer, OPL: Outer plexiform layer, ONL: Outer nuclear layer, ELM: External limiting membrane, IS/OS: Inner segment/outer segment junction, RPE: Retinal pigment epithelium (by Kanski J. 2011).

1.6 Limitations of TD-OCT

EA Swanson *et al.* mentioned that although the time domain Stratus OCT achieved high resolution images of the eye; the image quality was limited by the speed of image acquisition (**Fig. 4**). Also mentioned that in each successive axial scan, the axial movement of the eyes of the patients became increasingly important in the quality and precision of the image factor. After image acquisition, digital processing could eliminate axial movement artifacts, however, it could also introduce errors in the topography of the retina (Swanson EA, Izatt JA, He MR *et al.*, 1993). Image acquisition speed also limited the total number of cross-sectional images. The movement of the eyes, dry tear film and blinking were contributing to poor quality images with higher image acquisition time. As a result, the TD-OCT retina coverage was limited. Focal pathologies could not be detected in a B-scan determined by OCT, leading to sampling errors. Moreover, since the

OCT B-scan was limited (Ray R, Stinnet SS, Jaffe GJ, 2005; Sadda SR et al., 2006).

1.7 Spectral/Fourier-domain OCT (SD-OCT)

SD-OCT detection represents an advance in OCT technology that enables imaging speeds of >25,000 axial scans per second, or 50 times faster than TD-OCT. Spectral or Fourier domain OCT is so named because the interference spectrum of echo time delays of light is measured by a spectrometer and high-speed charged-coupled device camera (Fercher AF et al., 1995; Wojtkowski M et al., 2002; Nassif NA et al., 2004; Leitgeb RA et al., 2004; Srinivasan J et al., 2006).

Because the interference spectrum is composed of oscillations whose frequencies are proportional to the echo time delay, axial scan measurements can be obtained by calculating the Fourier transform. (A Fourier transform is a mathematical operation that extracts the frequency content of a signal). In contrast to TD detection, SD detection measures all echoes of light simultaneously, and the position of the reference arm does not need to be adjusted. The result is a significant improvement over time-domain OCT in sensitivity and image acquisition speed (Chen TC, Cense B, 2005) **(Fig. 5)**.

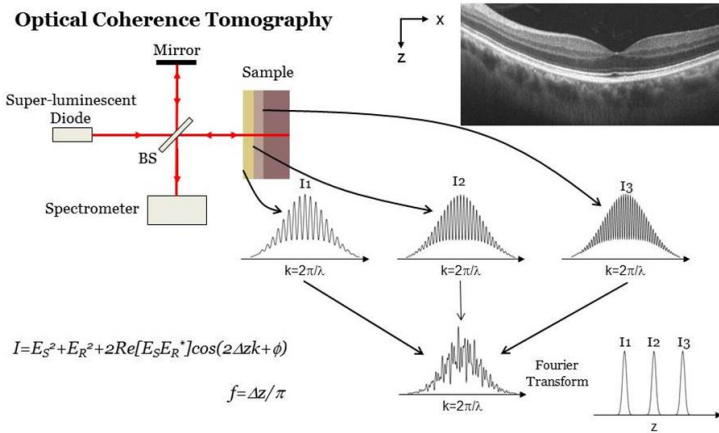


Fig.5: Multiple spectral/Fourier-domain OCT. Note the spectrometer and the Fourier transform in SD-OCT (by Graf 2009).

1.8 Limitations of SD-OCT

The disadvantage of spectral/Fourier domain detection is that detection sensitivity and image resolution depend on imaging depth because of limitations on spectrometer resolution.

1.9 Advantages of SD-OCT

One of the main advantages of the SD-OCT is that with the increase in speed of image acquisition, motion artifacts are minimized, resulting in images

of higher quality and finer discrimination of intraretinal layers. SD-OCT has the ability to acquire a large number of cross-sectional images quickly to improve the coverage of the retina and also has the ability to allow multiple scan OCT cross sections to be taken on in a pattern of dense plot to cover a large area of the retina (**Fig. 6**).

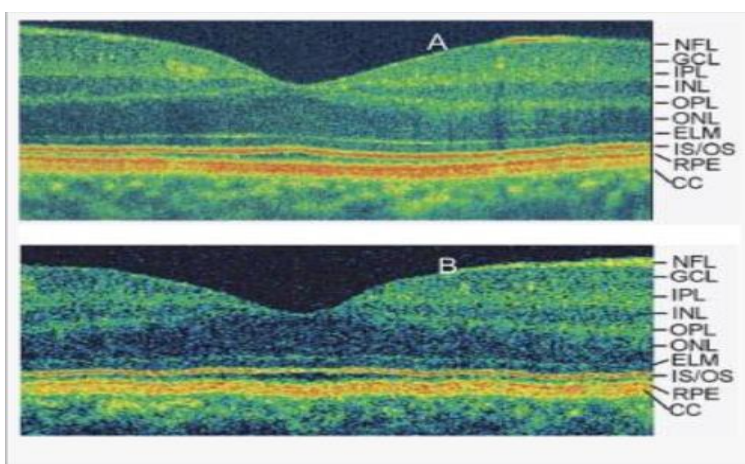


Fig.6: Comparison of TD to SD-OCT images. A normal macular scan acquired with SD-OCT (A). The same eye scanned with TD-OCT (B). Note the clear delineation of each retinal layer and the ability to clearly distinguish the inner segment/ outer segment junction of the photoreceptors from the retinal pigment epithelium in SD-OCT scans. NFL: Nerve fiber layer, GCL: Ganglion cell layer, IPL: Inner plexiform layer, INL: Inner nuclear layer, OPL: Outer plexiform layer, ONL: Outer nuclear layer, ELM: External limiting membrane, IS/OS: Inner segment/outer segment junction, RPE: Retinal pigment epithelium (by Yaqoob 2005).

1.10 Spectralis OCT

Spectralis OCT (Heidelberg Engineering, Heidelberg, Germany), is the newer SD-OCT that uses a significantly faster, non-mechanical technology.

Spectralis OCT measures simultaneously multiple wavelengths of reflected light across a spectrum, hence the name spectral domain. The system is 100 times faster than TD-OCT and acquires 40,000 A-scans per second with 5 μm optical, 3.9 μm digital axial resolution and 1.9mm scan depth. The increased speed and number of scans translates into higher resolution and a better chance of observing the diseases (Han IC, Jaffe GJ, 2009; Wolf-Schnurrbusch et al., 2009) **(Fig. 7)**.

High speed image acquisition is combined with custom TruTrack technology to actively track the eye during imaging. Tracking eye movement with simultaneous dual-beam imaging minimizes motion artifact, enables noise reduction and allows the instrument to precisely track change over time. This real-time eye tracking enables a highly repeatable alignment of OCT and fundus images that can be displayed either in grayscale or false color and allows acquisition of 1 to 100 B-scans at the same location, facilitating removal of speckle noise artifact. The result is point to point correlation

between the fundus and OCT scans, greater image detail and clarity, and more confident assessment of small changes (Wolf-Schnurrbusch et al., 2009).

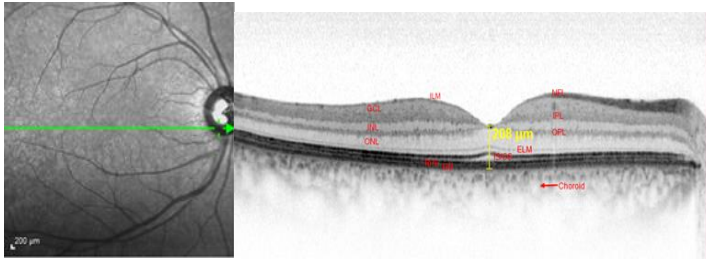


Fig. 7: Example of a normal eye image with the Spectralis OCT high resolution. (ILM: internal limiting membrane; NFL: nerve fiber layer; GCL: ganglion cell layer; IPL: inner plexiform layer; INL: inner nuclear layer; OPL: outer plexiform layer; ONL: outer nuclear layer; ELM: external limiting membrane; IS/OS: photoreceptor inner/outer segment junction; RPE: retinal pigment epithelium, BM: Bruch membrane).

1.11 OCT characteristics in Macula

The OCT-image closely approximates the histological appearance of the macula and, for this reason, it has been referred to as an in vivo optical biopsy. When light travels through the retinal tissue it can be reflected, scattered, or absorbed, and this creates the multilayered pattern of the retina (Drexler W, Fujimoto JG, 2008).

The first detected layer in most OCT scans is the ILM that appears as a hyper-reflective layer at the vitreoretinal interface. Occasionally, the posterior hyaloid can be seen above the ILM as a hyper-reflective layer. Within the retina, the RNFL, IPL and OPL are seen as hyper-reflective while the GCL and the nuclear layers are hypo-reflective. The retinal vessels may sometimes be seen on OCT images as circular hyper-reflective structures located in the inner retina, with a vertical shadow or reduced reflectivity extending into deeper layers (Drexler W, Sattmann H, 2003, Schuman JS, Puliafito CA, 2004; Spaide RF, Curcio CA, 2011).

Outside the central fovea, SD-OCT instruments typically resolve four bands in the outer retina. The innermost band has been attributed to the ELM. This band is typically thinner and fainter than the others. The second of the four bands has been commonly described to the boundary between the IS/OS of the photoreceptors and the third band is referred to as Verhoeff's membrane. The fourth hyper-reflective outer retinal band is attributed to the RPE, with potential contribution from Bruch's membrane and choriocapillaris, with abundant experimental and clinical evidence supporting this designation (Zawadzki RJ, Jones SM et al., 2005; Alam S, Zawadzki RJ et al., 2006; Srinivasan VJ, Ko TH et al., 2006;

Srinivasan VJ, Monson BK et al., 2008; Spaide RF, Curcio CA, 2011)
(Fig. 8).

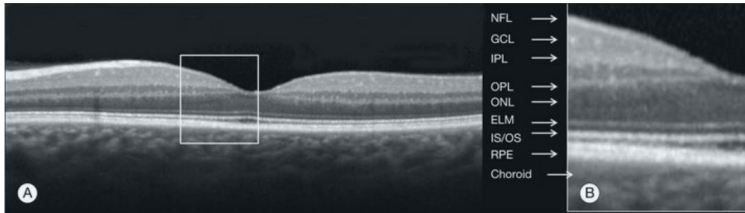


Fig. 8: (A) Example of a normal eye image with the Spectralis OCT high resolution. (B) Four hyper-reflective bands in the outer retina; ELM, IS/OS, Verhoeff's membrane and the RPE/Bruch's membrane complex. (NFL: nerve fiber layer; GCL: ganglion cell layer; IPL: inner plexiform layer; OPL: outer plexiform layer; ONL: outer nuclear layer; ELM: external limiting membrane; IS/OS: photoreceptor inner/outer segment junction; RPE: retinal pigment epithelium (by Ryan S. 2013).

1.12 OCT findings in Macular Diseases

Hard exudates are hyper-reflective lesions that look like hyper-reflective shades of neurosensory retina that completely block the reflections of the underlying retina. Thin hemorrhages are hyper-reflective, and if bleeding is thick, it can block the reflections of the underlying structures. Also epiretinal membrane (ERM), atrophy and all fibrotic lesions are hyper-reflective (Gupta V, 2004) **(Fig. 9).**

The hypo-reflective lesions are serous fluid that produces an optically empty space without

backscatter and pseudocysts characterized as a round or oval areas of low reflectivity in the layers of the retina (Gupta V, 2004) **(Fig. 10)**.

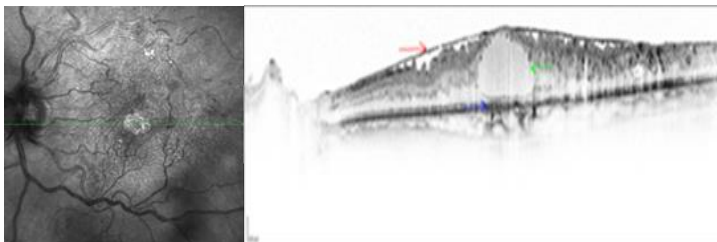


Fig. 9: Spectralis OCT 5mm horizontal line scan passing through the foveal center. Note the pseudocyst (green arrow) as an oval area of low reflectivity. Also, note the presence of hyper-reflective band ERM (red arrow) and a macula atrophy (blue arrow).

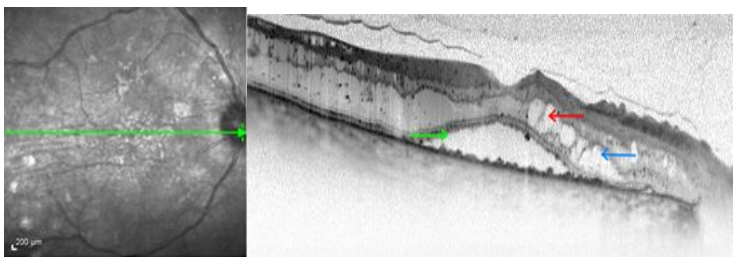


Fig. 10: Spectralis OCT 5mm horizontal line scan passing through the foveal center. Note the presence of hypo-reflective lesions; pseudocyst (red arrow) subretinal fluid (green arrow) and diffuse retinal thickness (blue arrow).

1.13 Pattern of OCT in Retinal Vascular Diseases

1.13.1 OCT in Diabetic Macular Edema (DME)

For the management of diabetic maculopathy, OCT is an important tool for assessing retinal pathology, including retinal thickness, DME, intraretinal exudates, vitreomacular interface abnormalities, subretinal fluid, and photoreceptor IS/OS junction abnormalities. OCT is also important in monitoring the response to treatment of DME by laser, intravitreal pharmacotherapies, and vitreoretinal surgery.

DME can be associated with diffuse retinal thickening, cystoid macular edema (CME), serous retinal detachment or subretinal fluid, and vitreomacular interface abnormality (Otani T et al., 1999; Kim BY et al., 2006; Soliman W et al., 2008).

Diffuse retinal thickening is usually defined as a sponge-like swelling of the retina with a generalized, heterogeneous, mild hypo-reflectivity compared with normal retina. CME is characterized by the presence of intraretinal cystoids areas of low reflectivity, which are typically separated by highly reflective septa (**Fig. 11**). Serous retinal detachment is defined on OCT as a focal elevation of neurosensory retina overlying a hypo-reflective, dome-shaped space (**Fig. 12**). The posterior border

of the detached retina is usually highly reflective, which helps to differentiate subretinal from intraretinal fluid. Vitreomacular interface abnormalities include the presence of ERMs, VMT, or both (Otani T et al., 1999).

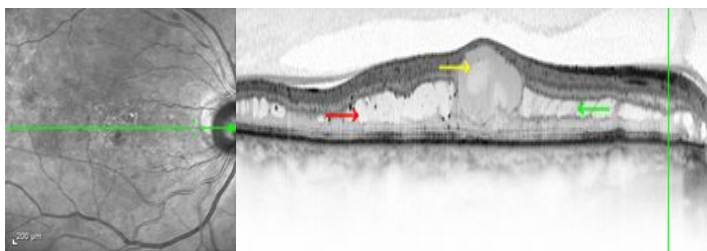


Fig. 11: Spectralis OCT 5mm horizontal line scan passing through the foveal center in an eye with DME. Note the large pseudocyst (yellow arrow), the sponge-like swelling of the retina (red arrow) and cystoid macular edema (green arrow) nasal to the fovea.

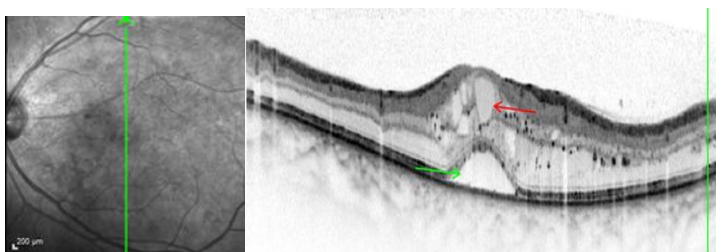


Fig. 12: Spectralis OCT 5mm vertical line scan passing through the foveal center in patient with DME. Note the presence of intraretinal cystoids areas of low reflectivity (red arrow), which are typically separated by highly reflective septa and a focal elevation of neurosensory retina overlying a hypo-reflective, dome-shaped space corresponding a serous retinal detachment (green arrow).

In the last decade, many agents like triamcinolone and anti-VEGF have been studied to treat DME. Michaelides M et al. mentioned that the OCT played an important role in determining the retinal thickness and the treatment response (Elman MJ et al., 2011; Michaelides M et al., 2010). Kim NR et al. reported that the treatment responses of each OCT pattern of DME are different. Patients with diffuse retinal thickening may achieve a greater reduction in retinal thickness and a greater improvement in visual acuity compared with patients exhibiting CME, subretinal fluid, or vitreomacular interface abnormality (Kim NR et al., 2009; Soliman W et al., 2008).

Fibrovascular proliferation in Proliferative Diabetic Retinopathy (PDR) can be visualized with OCT imaging as highly reflective preretinal bands anterior to the retinal surface. Diffuse retinal thickening, distortion, and irregularity of the retinal contour can also occur as a result of the contraction of these preretinal membranes. An associated traction retinal detachment may be observed as well (**Fig. 13**). OCT imaging is valuable in determining the extent of the tractional component as well as the presence of foveal involvement, assisting in the decision to intervene surgically (Haller JA et al., 2010).

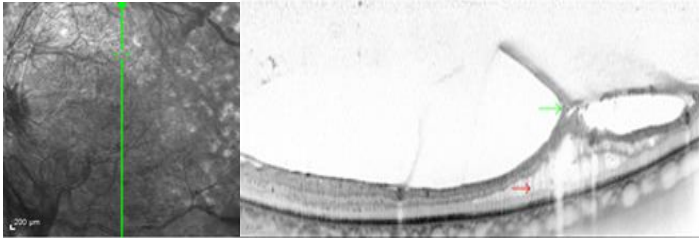


Fig. 13: Spectralis OCT: 5mm vertical line scan through the macula in a patient with PDR. Note the highly reflective preretinal band anterior to the retinal surface (green arrow) and the diffuse retinal thickening (red arrow), distortion and the irregularity of the retinal contour.

1.13.2 OCT in Branch Retinal Vein Occlusion (BRVO)

BRVO is the second most common vascular disease of the retina after DR, it is usually caused by a thrombus at arteriovenous crossings where a thickened artery compresses the underlying venous wall (Duker JS, Brown GL, 1989).

BRVO is usually seen in elderly patients, between 60-70 years old; this pathology is associated with hypertension in 50 to 70% of the cases, cardiovascular disease, diabetes mellitus, and open-angle glaucoma (Duker JS, Brown GL, 1989; Spaide RF et al., 2003).

OCT findings include CME (**Fig.14**), serous retinal detachment, ERMs, pseudoholes, lamellar holes

(Fig.15), and subhyaloid or preretinal hemorrhages in BRVO. A significant proportion of patients with occlusion of the retinal venous system have OCT evidence of CME and serous retinal detachment (Ota M et al., 2008; Shroff D et al., 2008; Ryan S et al., 2013).

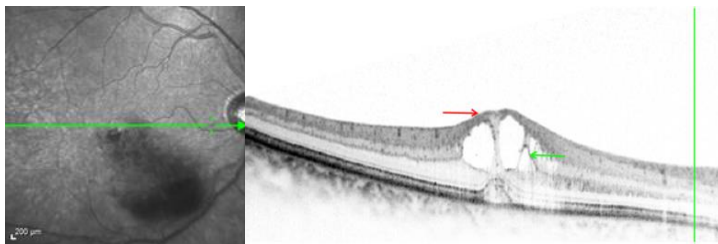


Fig. 14: Spectralis OCT 5mm horizontal line scan passing through the foveal center in patient with BRVO. Note the alteration in the foveal depression (red arrow) due to CME (green arrow) in an inferior-temporal retinal vein occlusion.

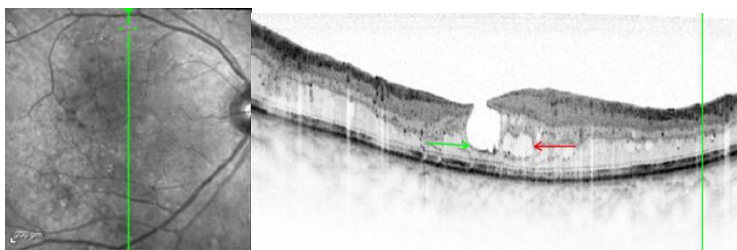


Fig. 15: BRVO associated with a lamellar macular hole, imaged by Spectralis OCT. Note the thin irregular foveal floor and split foveal edges (green arrow) accompanied with pseudocyst (red arrow).

1.13.3 OCT in Central Retinal Vein Occlusion (CRVO)

CRVO is usually caused by a thrombus in the area of the lamina cribrosa. It is associated with hypertension in 60% of patients. Usually seen in elderly patients over 50 years old and there is a slight male predilection (Hayreh SS, Zimmerman MB, 1994).

OCT plays a major role in studying macula in CRVO. In CRVO, the morphological findings visible in OCT include macular thickening, intraretinal cyst formation (**Fig.16**), lamellar macular holes, subretinal fluid accumulation, ERM and papilledema (Catier A et al., 2005; Lerche RC et al., 2001; Ozdemir H et al., 2005).

The quantification of macular edema is demonstrated on OCT as a changes on the foveal depression, hypo-reflective areas of fluid accumulation and pseudocysts. Intraretinal hemorrhages appear as focal areas of bright and hyper-reflective backscattering which partially shadow the reflections from the retinal pigment epithelium and choriocapillaris (Ryan S et al., 2013).

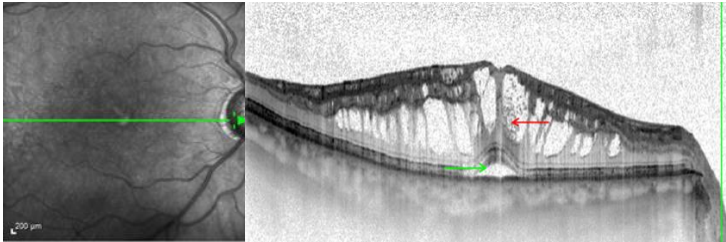


Fig 16: Spectralis OCT image shows a macular thickening, intraretinal cyst formation (red arrow) with a hypo-reflective subretinal fluid accumulation (green arrow) in CRVO.

1.13.4 Principles of the treatment of Retinal Vascular Diseases

Focal laser photocoagulation reduces the risk of moderate visual acuity loss by 50% of the patients with DME and reserved for the noncenter involved edema. Other treatments modalities for DME include intravitreal injection of anti-VEGF drugs and corticosteroids. In case of associated vitreomacular traction is a macular surgery recommended.

The response to various treatments modalities for macular edema is variable. Some patients show excellent visual improvement whereas others show only minimal response. Therefore OCT plays a pivotal role in quantitatively monitoring changes in retinal thickness after treatment such as intravitreal corticosteroid and anti-VEGF injection or

photocoagulation (Greenberg PB, Martidis A, 2002; Martinez-Jardon CS, Meza-de Regil A, 2005).

1.14 OCT in Vitreoretinal Interface Disorders

Abnormalities of the vitreoretinal interface are involved in the pathogenesis of several macular conditions. In idiopathic epiretinal membranes (ERMs), a layer of fibrotic tissue develops on the surface of the retina, usually after a posterior vitreous detachment. Contraction of this membrane can result in retinal distortion, leading to vision loss. In other conditions, such as vitreomacular traction syndrome (VMTS) or idiopathic macular hole (IMH), there are abnormal attachments between the vitreous and the retina. The resulting traction exerted on the retina causes anatomical alteration and subsequent visual loss.

1.14.1 Vitreomacular traction syndrome (VMTS)

VMTS results from persistent vitreoretinal adhesions after the development of partial posterior vitreous detachment (PVD). In normal eyes, as the vitreous liquefies due to age, it detaches from the macula. This natural progression has been demonstrated using OCT (Uchino E et al., 2001). In some eyes, due to the strong adhesion between the vitreous and

macula, the vitreous detaches peripherally, and continues to pull on areas of the macula. The vitreoretinal adhesions transmit tractional forces to the retina from the vitreous body, having the potential to cause tensile deformation (**Fig.17**), foveal cavitations, CME, limited macular detachment, or a macular hole (MH) (Schmidy WE et al., 1989; Jhonson MW, 2005).

In recent years OCT has been most beneficial in diagnosing VMTS and subsequently directing treatment of this condition.

Sulkes DJ et al. mentioned that in some people spontaneous resolution can occur with separation of the vitreous from the macula, leading to subsequent resolution of the intraretinal and subretinal fluid and restoration of normal vision (Sulkes DJ et al. 2000). However, in most eyes, VMTS may persist and intravitreal Ocriplasmin or vitrectomy may be an effective treatment option for patients with symptomatic VMTS. Consequently, OCT is useful in monitoring subtle changes in vitreoretinal adhesions and retinal architecture and assisting the treatment decision-making process (Yamada N, 2005; Witkin AJ et al. 2010).

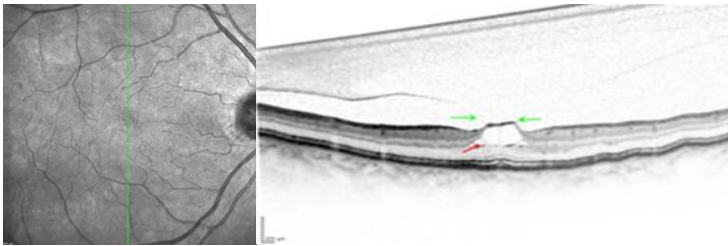


Fig. 17: Spectralis OCT shows persistent vitreous adhesion at the foveola (green arrows) causing tractional foveolar thickening with cyst-like spaces (red arrow). This type of vitreofoveolar traction is a subtle variant of the vitreomacular traction syndrome.

1.14.2 Epiretinal membrane (ERM)

ERM occurs in approximately 6% of patients over the age of 60, with incidence increasing with age (McCarty DJ et al., 2005). ERMs are idiopathic or secondary to an initiating event. Most idiopathic ERMs are thought to result from fibroglial proliferation on the inner surface of the retina secondary to a break in ILM occurring during PVD (Smiddy WE, Maguire AM et al, 1989). Secondary ERMs result from an already existing ocular pathology such as CRVO, BRVO, DR, uveitis, and retinal breaks with or without detachment (Appiah AP, Hirose T, 1989).

Glial cells, RPE cells, and myofibroblasts are shown to be mostly involved in ERM formation. (Smiddy WE, Maguire AM et al, 1989; Vinos SA et al.,1990). ERM may lead to loss of normal retinal anatomy, with the patient experiencing metamorphopsia, micropsia,

monocular diplopia, and decreased visual acuity. These symptoms vary in severity depending on the location, density, and contraction of the membrane.

Sometimes, ERMs can evolve into macular pseudoholes and ERMs are often seen in conjunction with idiopathic full-thickness macular holes (Schmidy WE, Michels RG et al., 1990).

OCT provides qualitative and quantitative information about the retinal anatomy, which can identify factors contributing to vision loss in patients with ERM.

On OCT, ERMs are seen as a highly reflective layer on the inner retinal surface (**Fig. 18**). In most eyes, the membrane is globally adherent to the retina (**Fig. 19**) but, in some cases, it can be separated from the inner aspect of the retina, which enhances its visibility by OCT. In this situation, it is usually distinguishable from a detached posterior hyaloid. Secondary effects of the membrane include loss of the normal foveal contour, increased retinal thickness, and the presence of cystoids changes, and these features may be observed in more advanced membranes.

OCT is also useful for monitoring changes in cases that are being observed and for documenting the

response to treatment in patients undergoing pars plana vitrectomy with membrane peeling.

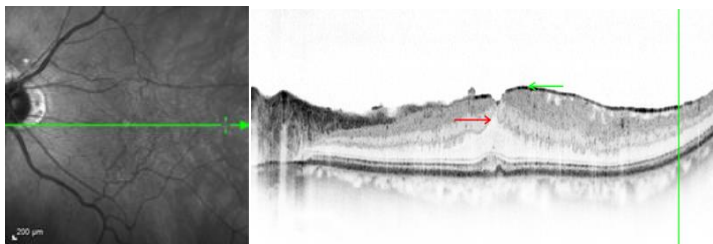


Fig. 18: Spectralis OCT shows the presence of hyper-reflective band (green arrow) at the vitreoretinal interface with traction on the underlying retina resulting in distortion of neurosensory retinal layers (red arrow).

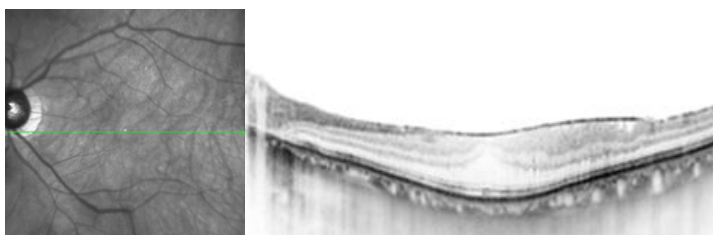


Fig. 19: Spectralis OCT shows a hyper-reflective band corresponding an epiretinal membrane globally adherent to the retina and a loss of the foveal depression.

1.14.3 OCT in Macular Holes

Idiopathic macular holes (IMHs) typically occur in the sixth to seventh decade of life with a 2: 1 female preponderance. Symptoms include decreased

visual acuity, metamorphopsia, and central scotoma. Bilateral involvement occurs in 15–20% of patients.

A full-thickness defect in the neural retina as seen with OCT can differentiate a true macular hole from a pseudohole, lamellar macula hole, or a macular cyst. Lamellar macula holes show an increased foveal pit contour with a thin outer neurosensory retina (**Fig. 20**). Macular pseudoholes are seen in the presence of a dense ERM with a central defect that overlies the foveal center, giving the ophthalmoscopic appearance of a true macular hole (Schumann JS, Puliafito CA, 2004) (**Fig. 21**).

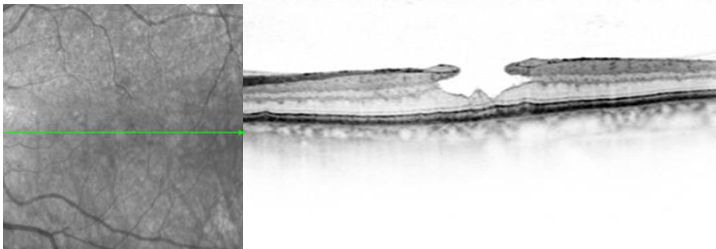


Fig. 20: Main Spectralis OCT features shows a lamellar hole. Note the horizontal splitting of the foveal edges, irregularity of the foveal base and thinning of the outer neurosensory retina.

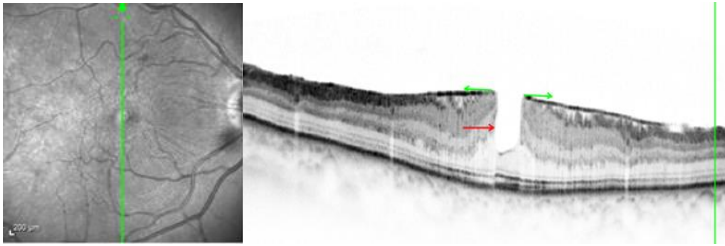


Fig. 21: Spectralis OCT features shows a pseudohole. Note the presence of a dense ERM (green arrows) with a steep configuration of the foveal edge (red arrow).

Gass described the stages of full-thickness MH formation based on biomicroscopic findings (Gass JD, 1995).

Stages 1 holes may be distinguished by a reduced or absent foveal pit and the presence of an optically clear space beneath the fovea, suggesting a foveolar detachment. Evidence of traction by the posterior hyaloid on the fovea may be present.

Stage 2 holes show a partial break in a surface of the retina with a small full-thickness loss of retinal tissue, <400 μm in size (**Fig. 22**).

Stage 3 holes have a full-thickness retinal dehiscence >400 μm in size with a complete break in the outer retinal tissue, and variable amounts of surrounding macular edema that increase retinal

thickness and decrease reflectivity in the outer retinal layers.

Stage 4 holes can be characterized by the complete loss of tissue $>400\ \mu\text{m}$ in size, and a complete detachment of the posterior vitreous (**Fig. 23**).

Stage 1 and 2 macular holes are very difficult to differentiate ophthalmoscopically and high resolution OCT images can help to classify them. Stage 2 often progresses to stage 3 with some visual loss; therefore, appropriate staging with OCT can help to determine when surgery is necessary (Gass JD, 1990).

Pars plana vitrectomy with and without ILM peeling has become the standard treatment for macular hole with anatomical success rates of 85–100% (Kelly NE, Wendy RT, 1991; Brooks HL JR, 2000). OCT can be used to confirm complete macular hole closure and restoration of the normal foveal contour.

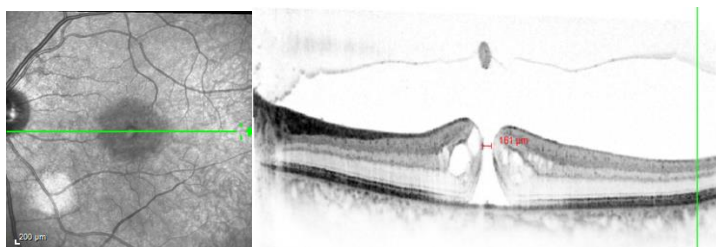


Fig. 22: Spectralis OCT shows a stage 2 macular hole. A small full-thickness loss of retinal tissue, $<400\ \mu\text{m}$ in size.

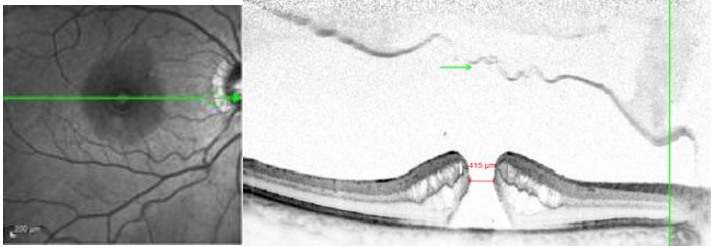


Fig. 23: Spectralis OCT shows a stage 4 macular hole. A full-thickness retinal defect $>400\mu\text{m}$ and a complete detachment of the posterior vitreous (green arrow).

1.15 OCT in Age-related macular degeneration (ARMD)

ARMD is a progressive degenerative disease of the retinal pigment epithelium, Bruch's membrane, and choriocapillaris. It is classified in two forms: non-neovascular (dry) and neovascular (wet or exudative). The non-neovascular form accounts for 80–90% of cases while the neovascular form accounts for 10–20% of cases, but was responsible for the majority of severe vision loss (80–90%) prior to the widespread use of vascular endothelial growth factor (VEGF) inhibitors. Occasionally, the dry form can develop into the wet (Friedman DS et al., 2004; Klein R et al., 2004).

ARMD is the most common cause of central vision defects in the elderly in the Western countries over 50 years population (Klein et al. 1998; Age Related Eye Disease Study Research Group 2000), It is estimated that approximately 30% of adults older than 75 years have some sign of ARMD and that approximately 10% of these patients have advanced stages of the disease.

Patients with advanced ARMD in one eye, or even moderate vision loss due to non-advanced ARMD in one eye, have about a 50% chance of developing advanced ARMD in the fellow eye within 5 years.

Risk factors include increasing age (>75 years of age), positive family history, cigarette smoking, hyperopia, hypertension, hypercholesterolemia, female gender, and cardiovascular disease; nutritional factors and light toxicity also play a role in pathogenesis. There may also be a genetic component to ARMD (Hirvela H et al., 1996; Vingerling JR et al. 1996).

1.15.1 Non-neovascular ARMD

Non-neovascular (dry) ARMD is characterized by abnormalities of the RPE, Bruch's membrane, and choriocapillaris. These abnormalities may be

asymptomatic or accompanied by compromised vision, and are considered to be the precursors of geographic atrophy (GA) and choroidal neovascularization (CNV) (Hirvela H et al., 1996; Vingerling JR et al. 1996).

Drusen appear clinically as focal white-yellow excrescences deep to the retina. They vary in number, size, shape, and distribution. The high-definition B-scans obtained with SD-OCT are useful to assess the ultrastructure of drusen and to evaluate for evidence of disruption of adjacent retinal layers (**Fig. 24**). Soft drusen are observed as focal elevations in the external, highly reflective band (RPE/choriocapillaris complex) consistent with the accumulation of amorphous material within or beneath Bruch's membrane (Sikorski BL et al., 2010; Spaide R, Curcio CA 2010) (**Fig. 25**).

In larger drusen or drusenoid retinal pigment epithelial detachments (PEDs), the RPE has a greater elevation with a dome-shaped configuration (Roquet W et al., 2004) (**Fig. 26**).

Larger drusen may often become confluent and can sometimes be accompanied by fluid accumulation under the retina in the absence of CNV (Sikorski BL et al., 2010). Recognition of this feature may avoid unnecessary treatment with anti-VEGF drugs.

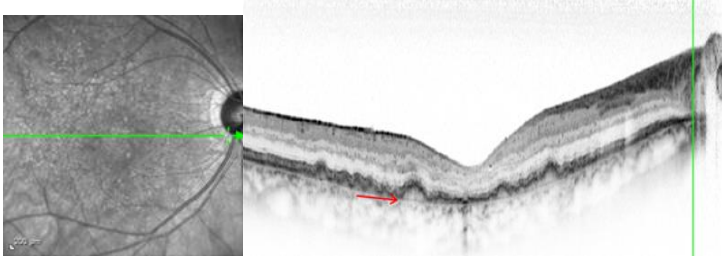


Fig. 24: Spectralis OCT shows the presence of drusen (red arrow) as a focal elevation between the retinal pigment epithelium and membrane Bruch's.

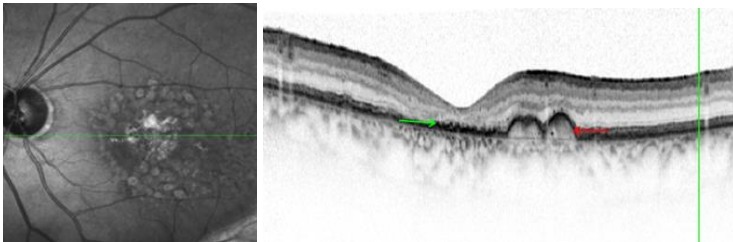


Fig. 25: Spectralis OCT shows the presence of large drusen (red arrow) and atrophy of the outer segments of the fovea (green arrow) in ARMD.

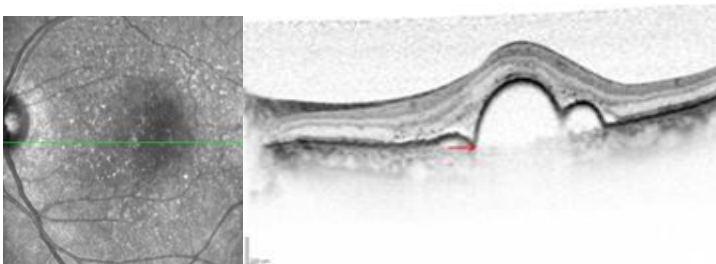


Fig. 26: Spectralis OCT shows a drusenoid RPE detachment (red arrow).

atrophy (GA) is seen clinically as one or more areas of hypopigmentation or depigmentation due to the absence of the underlying RPE. The deeper choroidal vessels are more readily visualized through the atrophic areas, and are accompanied by varying degrees of photoreceptor and choriocapillaris loss (**Fig. 27**). Associated retinal atrophy is seen as thinning or loss of the outer nuclear layer and the absence of ELM and IS/OS junctions (Fleckenstein M et al. 2008). The loss of photoreceptors often extends beyond the margins of GA, with the ELM and IS/OS junctions disappearing while bridging across the GA margin. Evaluation of these junctional zones may provide information about the pathogenesis of GA, and the role of RPE, photoreceptor, and choriocapillaris loss in the initiation and propagation of this condition (Bearelyly S et al. 2009). SD-OCT has been shown to be useful in detecting some of these morphologic alterations (**Fig. 27**).

Hyperpigmented RPE areas (hypertrophy or hyperplasia) in OCT show a high reflectivity from the RPE with shadowing of the reflections from the choroid.

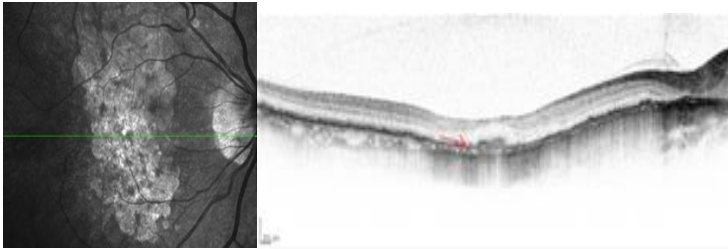


Fig. 27: Spectralis OCT shows a geographic atrophy (red arrow) in a patient with ARMD. Note the photoreceptor loss.

1.15.2 Neovascular ARMD

The neovascular (wet) form of ARMD is characterized by the overproduction of VEGF and the growth of abnormal vessels in the macular region. These vessels arise from the choroidal circulation and penetrate Bruch's membrane to form a fibrovascular tissue beneath or above the RPE, or these vessels may arise primarily from the retinal circulation. The presence of VEGF and abnormal vessels leads to structural changes in the retina and choroid with the accumulation of fluid within the retina, in the subretinal space, or under the RPE. Furthermore, this neovascular invasion may lead to significant disorganization and remodeling of the retina, resulting in the loss of the RPE and photoreceptors with the formation of a disciform scar (Green WR, 1999).

OCT is very useful in detecting intraretinal, subretinal, or sub-RPE fluid. In patients with active neovascular ARMD, OCT imaging can be used to establish baseline retinal thickness, and determine the extent of neovascularization, fluid involvement, and other lesion components (blood, fluid, pigment, and fibrosis).

The growth of neovascularization is often accompanied by VEGF-dependent leakage from both the mature vessels and the growing immature vessels (Schuman JS, Puliafito CA, 2004). Choroidal neovascularization is characterized by increased optical reflectivity of the RPE or disruption of the highly reflective band layer RPE/choriocapillaris (**Fig. 28**). Intraretinal edema appears as an area of low intraretinal reflectivity, which corresponds to intraretinal fluid accumulation and is consistent with an increased retinal thickness. Lipid exudation can also be present in patients with profuse intraretinal edema and appear as small hyper-reflective dots in the outer retina. The fluid may also accumulate in the space between the RPE and the neurosensory retina (**Fig. 28**).

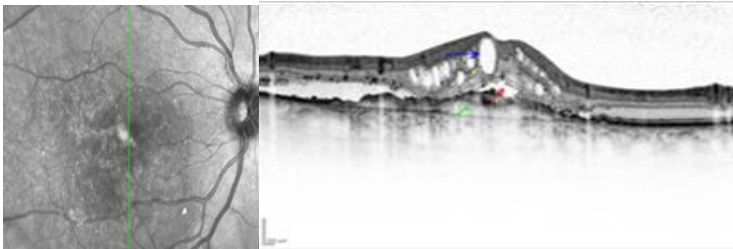


Fig. 28: Spectralis OCT shows the presence of choroidal neovascularization (green arrow), intraretinal fluid accumulation (red arrow) and cystoid macular edema (blue arrow) in ARMD.

A pigment epithelium detachment (PED) demonstrates an elevation of the reflective band corresponding to the RPE/choriocapillaris complex and shadowing of the reflections returning from the deeper choroid. In contrast, neurosensory retinal detachment appears as elevations of the sensory retina above an optically clear space (Fig. 29).

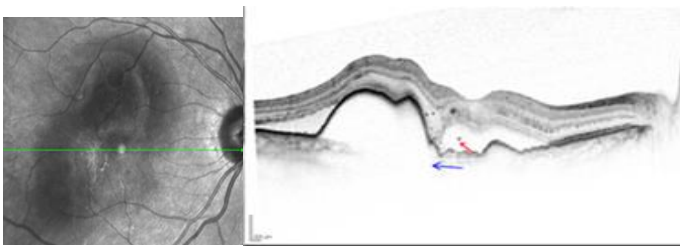


Fig. 29: Spectralis OCT shows the presence of PED (blue arrow), and neurosensory retinal detachment that appears as elevations of the sensory retina above an optically clear space (subretinal fluid accumulation) (red arrow) in ARMD.

Disciform scarring and subretinal fibrosis are the end stage of CNV. The vascular components of CNV typically regress as the lesion becomes less active, and the fibrous components typically increase, resulting in disciform scar formation. Clinically the scar appears as smooth, elevated white or gray tissue in the subretinal space and on OCT imaging the scar corresponds to a highly reflective outer retinal or subretinal lesion (Schuman JS, Pulliafito CA, 2004) **(Fig. 30)**.

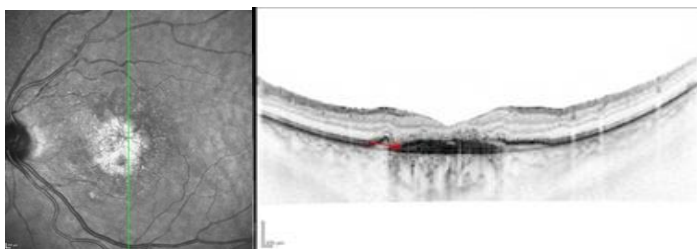


Fig. 30: Spectralis OCT shows the presence of disciform scarring (red arrow) as a highly reflective subretinal lesion between the retinal pigment epithelium and Bruch's membrane.

1.16.3 Treatment of ARMD

There are several types of treatments for ARMD. Argon laser photocoagulation is a therapy for cases where the CNV is extrafoveal. Photodynamic therapy (PDT) is a cold laser irradiation to specifically destroy the neo-vessels, particularly

subfoveal CNV. The Anti-VEGF agents are drugs that bind to and block the activity of VEGF (Bandello F, Battaglia Parodi M, Siemerink MJ et al, 2010). Currently, the intravitreal anti-VEGF application is the gold standard for the treatment of neovascular ARMD. The macular surgery is deserved for some complicated cases, such as large submacular hemorrhages in ARMD.

1.17 Anti-VEGF treatments

Even though the reasons and the clinic of these diseases are different, most of the vascular diseases of the retina and choroid are associated with exudative changes in the macula except epiretinal membrane. These changes are leading to damage of the photoreceptors and causing vision loss. New hopes in treating all of these diseases are the anti-VEGF therapy.

VEGF is a protein that occurs naturally within the body. Bodily tissues are thought to release this protein to signal the need for additional oxygen. Nearby blood vessels can sense the presence of this protein and in response, sprout and grow new blood vessels that extend into the VEGF releasing

tissue. This brings new pathways of blood supply into the oxygen needed tissue.

Many times the activity of VEGF is helpful, but for example after a CRVO, VEGF is thought to contribute to macular edema by increasing the permeability of the capillary walls, allowing fluids and proteins to make their way into the macular tissue. VEGF is also thought to be the culprit that stimulates the formation of the abnormal, fragile vessels of neovascularization.

Anti-VEGF agents are drugs that bind to and block the activity of VEGF (Bandello F, Battaglia Parodi M, Siemerink MJ et al., 2010).

1.17.1 Ranibizumab (Lucentis)

This is a recombinant humanized monoclonal antibody antigen-binding fragment (Fab) that neutralizes all known active forms of vascular endothelial growth factor A (VEGF-A), a protein that is believed to play a critical role in the formation of new blood vessels. Ranibizumab is an Anti-VEGF developed specifically for use in the eye. The usual dose of intravitreal injection is 0.5 mg in 0.05 ml.

Three main treatment strategies are currently adopted. The first strategy is a regular monthly injection that is the regimen adopted in initial major trials. Overall, around 95% of patients maintain vision regardless of lesion type, and 35–40% significantly improved, most markedly during the first 3 months. The second strategy is the three initial monthly injections followed by monthly review with re-injection when deterioration occurs as assessed by VA and OCT and the third strategy is the ‘treat and extend’ that administer three initial injections at monthly intervals and then gradually increasing the period between injections until deterioration is evident. If possible a tailored interval is determined for each patient. (Bandello F, Battaglia Parodi M, Schmidt-Erfurth U et al, 2010).

1.17.2 Bevacizumab (Avastin)

This is a recombinant humanized monoclonal antibody that produces angiogenesis inhibition by inhibiting VEGF-A. In contrast to ranibizumab (48 kDa), bevacizumab is a complete antibody (149 kDa). The indication is macula edema and proliferative (neovascular) eye diseases, particularly for CNV in ARMD (Bandello F, Battaglia Parodi M, Schmidt-Erfurth U et al, 2010). The usual dose of intravitreal injection is 1.25 mg/0.05 mL or 2.5 mg/0.1 mL. (Arevalo JF, et al. 2008).

According to the Comparison of Age-related Macular Degeneration Treatment Trials (CATT) study, there is no clinical significant difference or inferiority between ranibizumab and bevacizumab in treating patients with ARMD. (Martin DF et al., 2012).

1.17.3 Pegaptanib (Macugen)

Pegaptanib sodium was the first anti-VEGF agent approved by regulatory authorities for ocular treatment. Although offering visual outcomes superior to photocoagulation, the results are similar to outcomes with PDT, and use of pegaptanib is considerably less widespread than other anti-VEGF agents (Bandello F, Battaglia Parodi M, Schmidt-Erfurth U et al, 2010).

1.17.4 Aflibercept (Eylea)

Aflibercept is a novel VEGF inhibitor, with a high affinity for VEGF. It is a protein constructed by fusion of the second binding domain of the receptor VEGFR1 and the third binding domain of the receptor VEGFR2 to the crystalline portion of IgG1. This has resulted in aflibercept's having a significantly higher affinity in vitro to VEGF compared with both bevacizumab and ranibizumab (Holash J et al. 2002; Stewart MW, Rosenfeld PJ, 2008; Stewart MW, 2012; Bakall B et al. 2013).

2. Material and Methods

2.1 General objective:

Determine the agreement between the general ophthalmologist and retina specialist in the diagnosis and classification of macular diseases by high- definition spectral-domain optical coherence tomography (Spectralis OCT).

2.2 Hypothesis

Hypothesis (H1): There is statistically significant difference in agreement between the general ophthalmologist and the retina specialist to recognize findings by Spectralis OCT.

Null hypothesis (H0): There is no statistically significant difference in agreement between the general ophthalmologist and the retina specialist to recognize findings by Spectralis OCT.

2.3 Definitions

Degree of agreement: Is the concordance among raters. It gives a score of how much homogeneity, there is in the ratings given by judges.

Not in agreement: Is the discordance between raters.

Nongradable: No decision because of the poor image quality.

Limits of agreement: Refers to calculate the differences between each pair of observations of the two raters. The average of these differences is called bias and the reference range (mean + / - 1.96 x standard deviation) is termed limits of agreement.

2.4 Study population

After taken the approval by the Ethics committee das Institut für Klinische Epidemiologie und angewandte Biometrie der Eberhard Karls Universität zu Tübingen. We performed a retrospective chart review of patients who visited der Eberhard Karls, Universitäts-Augenklinik, Tübingen between August 2009 and September 2012. Clinical records of consecutive patients,

diagnosed with neovascular ARMD, BRVO, CRVO, BRVO, DME, and ERM that Spectralis SD-OCT examination with linear scan protocol were included in this study. In total, data of 500 patients were evaluated.

All patients underwent complete ophthalmic examination and Spectralis OCT. Fluorescein angiography and indocyanine green angiography were performed in some of the patients if needed. Using the digital chart system, list of the patients with predefined diseases were found.

2.5 Inclusion criteria

1. Patients with neovascular ARMD, BRVO, CRVO, DME and ERM.
2. Patients older than 18 years old.
3. Fundus photography and fluorescein angiography (except for eyes with ERM) at baseline.
4. Available Spectralis OCT examination of the macula.
5. Morphological abnormalities at the macula detected on the Spectralis OCT examination.

2.6 Exclusion criteria

1. Eyes having more than one disease affecting the macula (for example, neovascular ARMD and BRVO on the same eye).
2. The second eye of the included patients.
3. Eyes with poor quality of fundus photographs or fluorescein angiography.

2.7 Selection of the study population

After considering the inclusion and exclusion criteria, for each of the predetermined five diseases, 100 eyes of each disease were included into the analysis. All of the 500 consecutive eyes were selected by a senior ophthalmologist (FG) of the Department of Retina after checking the patient's charts and Spectralis OCT scans.

Eyes were selected if morphological abnormalities at the macula were seen on the Spectralis OCT examination.

2.8 Design

This study is transactional, correlational, and retrospective; because we analyze significant morphological findings (variables) that are presented in each disease into a single image at a time, also the relationship that exists between intra and interobserver.

2.9 Design description.

In September 2012, images (vertical and horizontal linear scans do Spectralis OCT) of the patient's first visit were selected by the general ophthalmologist (examiner 1). By that time the central retinal thickness (CRT) was measured in both images, determining the average value of the 500 eyes of 500 patients with the diagnosis categories noted above. After that the variables of the 5 groups were assessed, in addition to assessing the quality of the image by the OCT.

Between September 2012 and December 2012, the general ophthalmologist learned to use the Spectralis OCT in high resolution as well as, interpret and diagnose macular disorders during the clinical routine.

In December 2012, the second measurement of the CRT was repeated by the same general ophthalmologist; the same OCT image-scans were used as before.

In March 2013, the retina specialist (examiner 2), with an experience of performing and analyzing of the Spectralis OCT evaluated the CRT as well as the variables of the included eyes.

2.10. Sample size

For the analysis, we included into the study 500 images of 500 eyes (500 patients) with predefined macular diseases.

These were:

- 1- 100 eyes (100 patients) with age-related macular degeneration (ARMD).
- 2- 100 eyes (100 patients) with branch retinal vein occlusion (BRVO).
- 3- 100 eyes (100 patients) with central retinal vein occlusion (CRVO).
- 4- 100 eyes (100 patients) with diabetic macular edema (DME).
- 5- 100 eyes (100 patients) with epiretinal membrane (ERM).

2.10.1 Analyses of the OCT scans

In all patients, the macula was scanned in the horizontal and vertical meridians using the standard lineal protocol of Spectralis OCT. The CRT was calculated for each image using a 5mm length centered through the fovea, twice by general ophthalmologist (HT), in September 2012 and December 2012 and thereafter by the retina specialist (ML) in March 2013.

Data was obtained from the right eyes if both eyes fulfilled the inclusion criteria.

2.11 Evaluation method

2.11.1 Ophthalmologic examination

All patients had a general ophthalmological examination including best corrected visual acuity, biomicroscopy of the anterior segment, measurement of the intraocular pressure and funduscopy in mydriasis. All eyes had color fundus photography and Spectralis OCT. Fluorescein angiography and Indocyanine green angiography was performed if needed.

2.12 Examination protocol of the OCT

2.12.1 Preparation of the patient

After the eye examination, OCT was performed on patients with suspected macular alteration.

- 1- Patient data was given.
- 2- Pupillary dilation.
- 3- Positioning of the head of the patient (Supported of the front and chin).
- 4- IR+OCT of Spectralis.

Spectralis OCT examinations were performed by an ophthalmologist or technician.

2.12.2 Preparation of the OCT

OCT scans included in this Study were generated using Heidelberg Engineering, HTR-OCT Spectralis, and version 1.8.6.0. Heidelberg, Germany (**Fig.31**)



Fig. 31: Spectralis OCT (Heidelberg Engineering, Heidelberg, Germany).

2.12.3 Settings of Spectralis OCT

Eye: OD/OS

Angle: 0-90 grades

Focus: -10 to 10 Diopters

Sensitivity: >59

Power: IR 100%

Rate: 4.7 sec.

Resolution: High resolution

Application structures: Retina

Scan: Horizontal or vertical

ART: 100 Frames A-Scans: 1024 to 1536

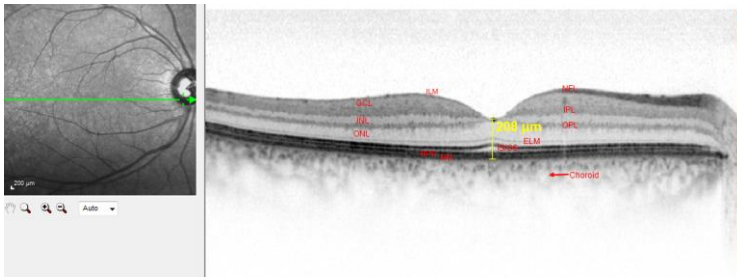


Fig. 32: Spectralis OCT horizontal line scan shows the layers of the retina and measurement of CRT. ILM: internal limiting membrane; NFL: nerve fiber layer; GCL: ganglion cell layer; IPL: inner plexiform layer; INL: inner nuclear layer; OPL: outer plexiform layer; ONL: outer nuclear layer; ELM: external limiting membrane; IS/OS: photoreceptor inner/outer segment junction; RPE: retinal pigment epithelium.

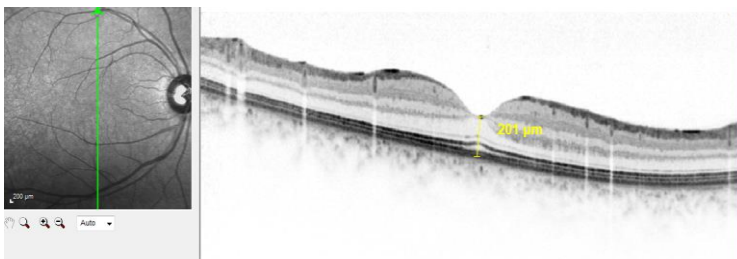


Fig. 33: Spectralis OCT vertical line scan shows CRT measurement from ILM to RPE/Bruch membrane complex.

The CRT was manually measured in all scans using the manual caliper tool built into the OCT software **(Fig. 32, 33)** twice by HT, in September 2012 and December 2012 and again by ML in March 2013. Both examiners were masked to any clinical, angiographic or functional status of the eyes when grading the scans.

CRT was defined as the interface between the dark vitreous and the bright reflection of the internal limiting membrane (ILM) and the outer retinal surface of the bright retinal pigment epithelium/Bruch's membrane complex at the fovea. Measurements were taken in the central 1mm of the OCT scans (Ian C, Han MD, Jaffe GJ, 2008) **(Fig. 32, 33)**.

In addition, all OCT scans were graded for the presence or absence of the following morphological findings: foveal depression, epiretinal membrane, vitreofoveolar traction, pseudocyst, splitting, verticalisation of the foveal edge, macular hole, pseudomacular hole, lamellar macular hole, neurosensory detachment of the retina, retinal pigment epithelium detachment, external limiting membrane, photoreceptors inner and outer segments.

2.13 Artifacts and Gradability of the images

Each horizontal and vertical line scans were reviewed in terms of the gradability. Scans with significant image artifacts resulting in reliable thickness measurements of the retina were excluded. Reasons for scan exclusion included weak saturated scans where the boundaries of the retina or intraretinal morphology could not be identified adequately and off-center scans which were not centered within the foveal pit.

For patients with multiple acceptable scans per eye in the same clinic visit, one scan per eye was chosen at random to be included in the study.

2.14 Color fundus photography, Fluorescein angiography and Indocyanine green angiography

All patients had color fundus photography of both eyes. Some patients underwent fluorescein and indocyanine green angiography at the first presentation to diagnose the macular pathology.

These examinations were performed by skilled photographers at the imaging department.

2.15 Data analysis

A coding scheme was conducted to evaluate the morphological findings (variables), as well as for the database.

Abbreviation	Text	Type of scale	Ranges of values	Unit	Role
ID	Number of patient	Numeric	1-500	-	Identification
Examination	Examination	Numeric	1.September H.T 2.December H.T 3.March M.L		
Age	Age of patient	Statistic	30-100	Years	Age
Gender	Gender	Numeric	M for Men W for Women	-	Gender
Diagnosis	Diagnosis of the eye	Numeric	1. BRVO 2. CRVO 3. DME 4. ARMD 5. ERM	-	Diagnose
Study eye	Study eye	Numeric	L for Left R for right	-	Eye
Exam Date	Exam Date	Statistic	15.03.2008 – 16.03.2013	Date	
CRT_FD_H	Central retinal thickness of the fovea (horizontal scan of the study eye)	Statistic	0 – 1300	Mm	Microns
Quali_OCT	Quality of the OCT	Numeric	0-Good 1-Bad	-	Quality

			2-No assessable		
CRT_FD_V	Central retinal thickness of the fovea (vertical scan of the study eye)	Statistic	0 – 1300	Mm	Microns
Quali_OCT	Quality of the OCT	Numeric	0-Good 1-Bad 2- No assessable	-	Quality
CRT_FD_D	Central retinal thickness of the fovea (Average)	Statistic	0 – 1300	Mm	Microns
Fo_De	Foveal Depression (of the study eye)	Numeric	0-Normal 1-Abnormal 2- No assessable	-NL -ANL -N/A	
Quali_OCT	Quality of the OCT	Numeric	0-Good 1-Bad 2- No assessable	- - N/A	Quality
ERM	Epiretinal Membrane (of the study eye)	Numeric	0-No 1-Yes 2- No assessable	- - N/A	
Quali_OCT	Quality of the OCT	Numeric	0-Good 1-Bad 2- No assessable	- - N/A	Quality
VFT	Vitreofoveal traction (of the study eye)	Numeric	0-No 1-Yes 2- No assessable	- - N/A	
Quali_OCT	Quality of the OCT	Numeric	0-Good 1-Bad 2- No assessable	- - N/A	Quality
Pseudocyst	Pseudocyst	Numeric	0-No	-	

	(of the study eye)		1-Yes 2- No assessable	- N/A	
Quali_OCT	Quality of the OCT	Numeric	0-Good 1-Bad 2- No assessable	- - N/A	Quality
Splitting	Splitting (of the study eye)	Numeric	0-No 1-Yes 2- No assessable	- - N/A	
Quali_OCT	Quality of the OCT	Numeric	0-Good 1-Bad 2- No assessable	- - N/A	Quality
Verticalisation	Walls of the foveal verticalisation (of the study eye)	Numeric	0-No 1-Yes 2- No assessable	- - N/A	
Quali_OCT	Quality of the OCT	Numeric	0-Good 1-Bad 2- No assessable	- - N/A	Quality
MH	Macular Hole (of the study eye)	Numeric	0-No 1-Yes 2- No assessable	- - N/A	
Quali_OCT	Quality of the OCT	Numeric	0-Good 1-Bad 2- No assessable	- - N/A	Quality
PSM	Pseudomacular Hole (of the study eye)	Numeric	0-No 1-Yes 2- No assessable	- - N/A	
Quali_OCT	Quality of the OCT	Numeric	0-Good 1-Bad 2- No assessable	- - N/A	Quality
LMH	Lamellar Macular Hole (of the study eye)	Numeric	0-No 1-Yes 2- No assessable	- - N/A	
Quali_OCT	Quality of	Numeric	0-Good	-	

	the OCT		1-Bad 2- No assessable	- N/A	Quality
NSD	Neurosensory detachment (of the study eye)	Numeric	0-No 1-Yes 2- No assessable	- - N/A	
Quali_OCT	Quality of the OCT	Numeric	0-Good 1-Bad 2- No assessable	- - N/A	Quality
PED	Pigment epithelial detachment (of the study eye)	Numeric	0-No 1-Yes 2- No assessable	- - N/A	
Quali_OCT	Quality of the OCT	Numeric	0-Good 1-Bad 2- No assessable	- - N/A	Quality
LMO	Limiting membrane outer(of the study eye)	Numeric	0-Normal 1-Abnormal 2- No assessable	-NL -ANL -N/A	
Quali_OCT	Quality of the OCT	Numeric	0-Good 1-Bad 2- No assessable	- - N/A	Quality
IS/OS	Inner and outer segment junction	Numeric	0-Normal 1-Abnormal 2- No assessable	-NL -ANL -N/A	
Quali_OCT	Quality of the OCT	Numeric	0-Good 1-Bad 2- No assessable	- - N/A	Quality

2.16 Variables

Of the 5 groups of diseases 13 morphological findings (variables) were obtained and analyzed.

Definitions of the morphological findings (variables):

- 1. Foveal depression:** It is an excavation diameter of 1.5mm which corresponds to a slightly concave curvature on OCT image. An irregularity, a concavity or a convexity in an exaggerated foveal area could be suggestive to pathology.
- 2. Epiretinal membrane:** It is visible as a highly reflective layer on the inner retinal surface on OCT.
- 3. Vitreofoveolar traction:** It is characterized by the adhesion between the posterior vitreous and fovea.
- 4. Pseudocyst:** It is characterized as a round or oval areas of low reflectivity in the layers of the retina.
- 5. Splitting:** The edges of the fovea are split by a cleft between the inner and outer retina.
- 6. Verticalisation:** The edges of the fovea have a vertical appearance.

- 7. Macular hole:** It is characterized by an absence of foveal tissue.
- 8. Pseudomacular hole:** It is characterized by a steepened foveal pit combined with thickened foveal edges, verticalisation of the foveal slope and a small foveal pit diameter.
- 9. Lamellar macular hole:** It is characterized by a thin irregular foveal floor, split foveal edges and a near normal perifoveal retinal thickness.
- 10. Neurosensory detachment of the retina:** It is a separation that occurs between RPE and the photoreceptors.
- 11. Pigment epithelium detachment:** It is a separation that occurs between RPE and Bruch's membrane.
- 12. External limiting membrane:** It is the junctions between photoreceptor cells and Müller cells.
- 13. Photoreceptors inner and outer segments:** Are the layers of rods and cones (photoreceptors cells).
(Haouchine B, Massin P, Tadayoni R, et al. 2004;
Chang LK, Fine HF, Spaide RF, et al., 2008)

2.17 Statistical analysis

For the statistical analysis, we consulted das Institut für Klinische Epidemiologie und angewandte Biometrie der Eberhard Karls Universität zu Tübingen.

Statistical analysis was performed using JMP software version 10.0 (SAS Institute, Inc., Cary, NC) and Microsoft Office Excel 2010 ® (Microsoft Corp., Seattle, WA).

Tables and graphs from JMP 10 program were used to determine demographic data.

For the statistical analysis of central retinal thickness (CRT) we used the individual differences analysis (Bland-Altman method) so it measured the concordance between 2 systems of measurement and it represented graphically the differences between 2 measurements front the mean.

Paired t tests were used to compare CRT measurements differences between observers and P values less than 0.05 were considered statistically significant.

For the analysis of the distribution of variables, we used the method fit Y by X. This method evaluates the relationship between variables. Thus, we found

the degree of agreement between the HT1-HT2 (intraobserver) and HT1-ML3, HT2-LM3 (interobserver) in 500 images of eyes of 500 patients (one eye per person).

2.18 Description of activities

Description of activities															
Months \ Activities	1	2	3	4	5	6	7	8	9	10	11	12	13	14	15
Selection of photographs	X	X	X												
Measurement of CRT and V by HT			X	X	X	X	X	X							
Measurement of CRT and V by ML									X	X					
Capture results in database											X				
Analysis of results											X	X	X		
Write results												X	X	X	X

*CRT= Central retinal thickness. *V= variables.

3. Results

3.1 Demographic data

For this study, we selected the images of the patients who met the inclusion and exclusion criteria of the Eberhard-Karls, Universitäts-Augenklinik, Tübingen. For the patients, we retrospectively reviewed the files of 500 eyes of 500 consecutive patients (one eye per person) who were examined between August 2009 and September 2012 and were diagnosed as having neovascular ARMD, BRVO, CRVO, DME and ERM.

The demographic analysis was conducted based on the number of patients. 274 were male and 226 female, the left eyes in 253 patients were included, while the right eyes were from 247 patients. The mean age was 73.2 years. (RANGE, 68 to 79) **(Table 1).**

Eyes, n (%)	
Right	247 (49.4)
Left	253 (50.6)
Total	500 (100)

Gender, n (%)	
Men	274 (54.8)
Women	226 (45.2)
Age (y)	
Mean ± SD	73.2 ± 10.5
Range	68-79

Table 1. Demographics data of patients with macular diseases.
n= Number of patients.

Of the 500 images, a second selection was performed. 307 images were included in the study of CRT and 193 were discarded due to lack of concordance between observers (**Table 2**).

DIAGNOSIS	N	HT1- HT2	HT1- ML3	HT2- ML3	HT1- HT2- ML3
ARMD	100	82	73	74	72
BRVO	100	87	54	55	54
CRVO	100	81	55	57	55
DME	100	91	53	55	53
ERM	100	92	74	76	73
Total	500	433	309	317	307
Total %	100 %	86.6 %	61.8 %	63.4 %	61.4 %

Table 2. Gradability of OCT-images by observers.

* Imaging was assessed by both observers in 3 examinations.

HT1= First examination by HT, HT2= Second examination by HT, ML3= First examination by ML. ARMD= Age-related macular degeneration, BRVO= Branch retinal vein occlusion, CRVO= Central retinal vein occlusion, DME= Diabetic macular edema, ERM= Epiretinal membrane, n= Number of patients.

3.2 Results of CRT in macular diseases

A simple graphical method for assessing the agreement between two measurement systems was proposed by Bland and Altman. This method was used to analyze the difference between two measurements against their mean. (Altman DG, Bland JM, 1983; Bland JM, Altman DG, 1986). Therefore, to measure the CRT of each disease, the average values of the vertical line scanning and horizontal line scanning by HT (general ophthalmologist) and ML (retina specialist) were used respectively. After having been obtained, the 307 images, each diagnosis was analyzed separately by both observers.

3.3 Intraobserver agreement in macular diseases (HT1-HT2).

According to the intraobserver analysis between HT1 and HT2 the mean differences of the CRT were very similar, resulting in 1.67 to 9.50 μ m. The coefficient correlation (CC) was 0.73 to 0.98. The 95% confidence interval (CI) was in ARMD (13.24; -18.87 μ m); BRVO (22.38;-3.25 μ m); CRVO (33.53; -19.89 μ m); DME (11.29; -7.94 μ m); ERM (29.48;-23.34 μ m); and the P-value of all of them was

greater than 0.05 statistically insignificant (**Table 3**) (**Graphic 1**).

Therefore no significant differences were observed within 3 months by HT.

Diagnosis	n	Mean CRT HT1 (µm)	Mean CRT HT2 (µm)	Mean Difference (µm)	Correlation (CC)	95 % (CI) (µm)	*P-value (P>0.05)
ARMD	72	230.99	228.18	2.81	0.79	13, -18	0.72
BRVO	54	347.97	338.40	9.56	0.95	22, -3	0.14
CRVO	55	598.22	591.40	6.81	0.93	33, -19	0.61
DME	53	408.38	406.70	1.67	0.98	11, -7	0.72
ERM	73	293.24	290.17	3.06	0.73	29, -23	0.81

Table 3. Intraobserver agreement in macular diseases.

HT1= First examination by HT, HT2= Second examination by HT. ARMD= Age-related macular degeneration, BRVO= Branch retinal vein occlusion, CRVO= Central retinal vein occlusion, DME= Diabetic macular edema, ERM= Epiretinal membrane, n= Number of patients. CC= Coefficient correlation, CI= Confidence interval, µm= Microns.

*P: paired t tests of mean CRT measurements between Intraobserver.

3.4 Interobserver agreement in macular diseases: first analysis (HT1-ML3)

In the interobserver analysis 307 images were analyzed by HT1 and ML3, obtaining a mean difference ranged from 1.88 to 32.27 µm. The CC between the two observers ranged from 0.74 to 0.97. The 95% CI was in ARMD (17.24; -21.00 µm);

BRVO (43.62; 8.76 μm); CRVO (36.23; -13.27 μm); DME (27.25; 2.38 μm); ERM (50.34; 14.19 μm); and the P-value was statistically significant for DME ($P<0.02$), BRVO ($P<0.004$) and ERM ($P<0.0007$) but not in ARMD ($P=0.84$) and CRVO ($P=0.35$) **(Table 4) (Graphic 2).**

Diagnosis	n	Mean CRT HT1 (μm)	Mean CRT ML3 (μm)	Mean Difference (μm)	Correlation (CC)	95 % (CI) (μm)	*P-value ($P>0.05$)
ARMD	72	230.99	232.87	1.88	0.74	17, -21	0.84
BRVO	54	347.97	321.78	26.19	0.91	43, 8	0.004
CRVO	55	598.22	586.74	11.48	0.94	36, -13	0.35
DME	53	408.38	393.56	14.81	0.97	27, 2	0.02
ERM	73	293.24	260.97	32.27	0.82	50, 14	0.0007

Table 4. Interobserver agreement in macular diseases: first analysis. HT1= First examination by HT, ML3= First examination by ML. ARMD= Age-related macular degeneration, BRVO= Branch retinal vein occlusion, CRVO= Central retinal vein occlusion, DME= Diabetic macular edema, ERM= Epiretinal membrane, n= Number of patients. CC= Coefficient correlation, CI= Confidence interval, μm = Microns. *P: paired t tests of mean CRT measurements between Interobserver.

3.5 Interobserver agreement in macular diseases: second analysis (HT2-ML3)

In Bland-Altman analysis, interobserver mean difference ranged from 4.66 to 29.20 μm and CC ranged from 0.67 to 0.97. The 95% CI was in ARMD

(5.49; -14.82 μm); BRVO (31.69; 1.56 μm); CRVO (20.40; -11.08 μm); DME (28.23; -1.95 μm); ERM (55.19; 3.21 μm). An analysis of variance used for repeated measurement was statistically significant for BRVO ($P < 0.03$) and ERM ($P < 0.02$) but did not show significant difference in ARMD ($P = 0.36$), CRVO ($P = 0.55$), and DME ($P = 0.08$).

Therefore we can determine which of the five macular diseases had an agreement. These were ARMD, BRVO and DME but not CRVO, and ERM between observers (**Table 5**) (**Graphic 3**).

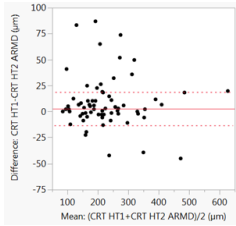
Diagnosis	n	Mean CRT HT2 (μm)	Mean CRT ML3 (μm)	Mean Difference (μm)	Correlation (CC)	95 % (CI) (μm)	*P-value ($P > 0.05$)
ARMD	72	228.18	232.87	4.69	0.93	5, -14	0.36
BRVO	54	338.40	321.78	16.62	0.93	31, 1	0.03
CRVO	55	591.40	586.74	4.66	0.97	20, -11	0.55
DME	53	406.70	393.56	13.13	0.95	28, -1	0.08
ERM	73	290.17	260.97	29.20	0.67	55, 3	0.02

Table 5. Interobserver agreement in macular diseases: second analysis.

HT1= First examination by HT, ML3= First examination by ML. ARMD= Age-related macular degeneration, BRVO= Branch retinal vein occlusion, CRVO= Central retinal vein occlusion, DME= Diabetic macular edema, ERM= Epiretinal membrane, n= Number of patients. CC= Coefficient correlation, CI= Confidence interval, μm = Microns.

*P: paired t tests of mean CRT measurements between Interobserver.

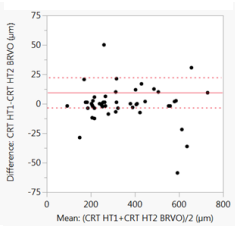
ARMD



Mean difference= 2.81 µm

95% CI= 13.24; -18.87 µm

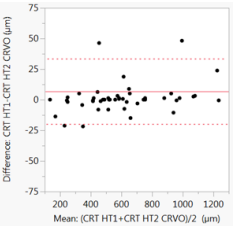
BRVO



Mean difference= 9.56 µm

95% CI= 22.38; -3.25 µm

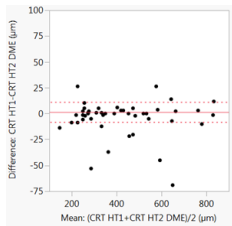
CRVO



Mean difference = 6.81 µm

95% CI= 33.53; -19.89 µm

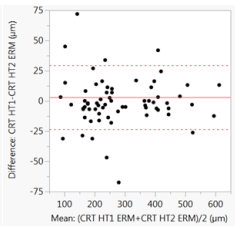
DME



Mean difference = 1.67 µm

95% CI= 11.29; -7.94 µm

ERM



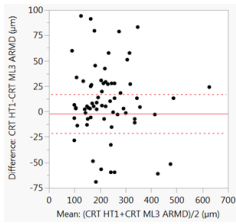
Mean difference = 3.06 µm

95% CI= 29.48; -23.34 µm

Graphic 1: Central retinal thickness between intraobserver in macular diseases.

Bland-Altman analysis showing the degree of agreement between intraobserver (HT1-HT2) in 5 different macular diseases. 95% CI= Confidence interval, CRT= Central retinal thickness, ARMD= Age-related macular degeneration, BRVO= Branch retinal vein occlusion, CRVO= Central retinal vein occlusion, DME= Diabetic macular edema, ERM= Epiretinal membrane, HT1= First examination by HT, HT2= Second examination by HT.

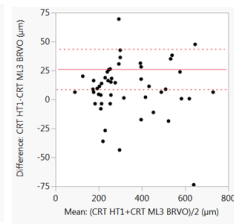
ARMD



Mean difference = 1.88 μm

95% CI = 17.24; -21.00 μm

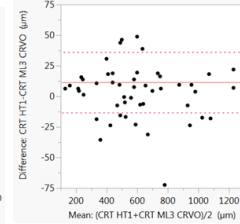
BRVO



Mean difference = 26.19 μm

95% CI = 43.62; 8.76 μm

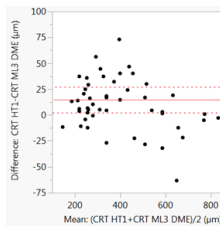
CRVO



Mean difference = 11.48 μm

95% CI = 36.23; -13.27 μm

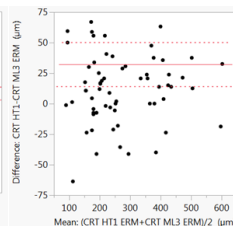
DME



Mean difference = 14.81 μm

95% CI = 27.25; 2.38 μm

ERM



Mean difference = 32.27 μm

95% CI = 50.34; 14.19 μm

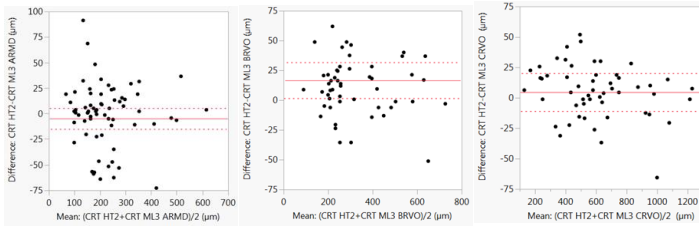
Graphic 2. Central retinal thickness between interobserver in macular diseases.

Bland-Altman analysis showing the degree of agreement between interobserver (HT1-ML3) in 5 different macular diseases. 95% CI= Confidence interval, CRT= Central retinal thickness, ARMD= Age-related macular degeneration, BRVO= Branch retinal vein occlusion, CRVO= Central retinal vein occlusion, DME= Diabetic macular edema, ERM= Epiretinal membrane, HT1= First examination by HT, ML3= First examination by ML.

ARMD

BRVO

CRVO



Mean Difference= 4.69 μm

Mean Difference= 16.62 μm

Mean Difference= 4.66 μm

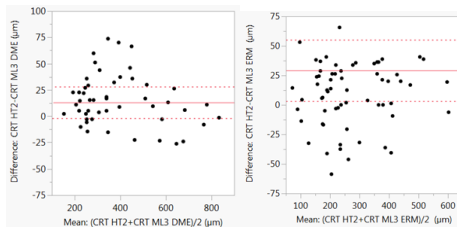
95% CI= 5.49; -14.82 μm

95% CI= 31.69; 1.56 μm

95% CI= 20.40; -11.08 μm

DME

ERM



Mean Difference= 13.13 μm

Mean Difference= 29.20 μm

95% CI= 28.23; -1.95 μm

95% CI= 55.19; 3.21 μm

Graphic 3. Central retinal thickness between interobserver in macular diseases.

Bland-Altman analysis showing the degree of agreement between interobserver (HT1-ML3) in 5 different macular diseases. 95% CI= Confidence interval, CRT= Central retinal thickness, ARMD= Age-related macular degeneration, BRVO= Branch retinal vein occlusion, CRVO= Central retinal vein occlusion, DME= Diabetic macular edema, ERM= Epiretinal membrane, HT2= Second examination by HT, ML3= First examination by ML.

3.6 Results of morphological findings (variables)

For the analysis of the distribution of variables, we used the method fit Y by X because this method evaluates the relationship between two variables. In this method we found the degree of agreement of 13 morphological findings between HT1-HT2 (intraobserver) and HT1-ML3, HT2-LM3 (interobserver) in 500 images of eyes of 500 patients (one eye per person) (Tables 6 to 18).

		Fo_De1			
Count		0	1	2	
Total %					
Fo_De2	0	59	23	3	85
	1	11.80	4.60	0.60	17.00
	2	56	304	18	373
	Total	11.20	60.80	2.60	74.60
Fo_De3	0	4	9	29	42
	1	0.80	1.80	5.80	8.40
	2	119	336	45	500
	Total	23.80	67.20	9.00	

		Fo_De1			
Count		0	1	2	
Total %					
Fo_De3	0	20	10	1	31
	1	4.00	2.00	0.20	6.20
	2	92	241	28	361
	Total	18.40	48.20	5.60	72.20
Fo_De3	0	7	85	16	108
	1	1.40	17.00	3.20	21.60
	2	119	336	45	500
	Total	23.80	67.20	9.00	

		Fo_De2			
Count		0	1	2	
Total %					
Fo_De3	0	12	17	2	31
	1	2.40	3.40	0.40	6.20
	2	68	265	28	361
	Total	13.60	53.00	5.60	72.20
Fo_De3	0	5	91	12	108
	1	1.00	18.20	2.40	21.60
	2	85	373	42	500
	Total	17.00	74.60	8.40	

a- Agreement (HT1-HT2): 78.4% b- Agreement (HT1-ML3): 55.2% c- Agreement (HT2-ML3): 57.8%

Table 6. Result of Foveal depression (Fo_De). Spectralis OCT findings: Fo_De1= Foveal depression analyzed by HT (first examination), Fo_De2= Foveal depression analyzed by HT (second examination), Fo_De3= Foveal depression analyzed by ML. 0- Foveal depression was normal, 1-Foveal depression was abnormal, 2- Foveal depression was not assessable. Red= Agreement, Blue=Not Agreement, Purple= Nongradable OCT Image.

		ERM 1			
Count		0	1	2	
Total %					
ERM2	0	306	45	10	365
	1	61.20	9.30	2.00	73.00
	2	12	76	5	93
	Total	2.40	15.20	1.00	18.60
ERM3	0	9	4	29	42
	1	1.80	0.80	5.80	8.40
	2	327	129	44	500
	Total	65.40	25.80	8.80	

		ERM 1			
Count		0	1	2	
Total %					
ERM3	0	111	7	8	127
	1	22.20	1.40	1.80	25.40
	2	147	96	16	259
	Total	29.40	19.20	3.20	51.80
ERM3	0	69	26	19	114
	1	13.80	5.20	3.80	22.80
	2	327	129	44	500
	Total	65.40	25.80	8.80	

		ERM 2			
Count		0	1	2	
Total %					
ERM3	0	110	5	12	127
	1	22.00	1.00	2.40	25.40
	2	176	69	15	259
	Total	35.20	13.60	3.00	51.80
ERM3	0	79	20	15	114
	1	15.80	4.00	3.00	22.80
	2	365	93	42	500
	Total	73.00	18.60	8.40	

a- Agreement (HT1-HT2): 82.2% b- Agreement (HT1-ML3): 45.2% c- Agreement (HT2-ML3): 38.6%

Table 7. Result of Epiretinal membrane (ERM).

Spectralis OCT findings: ERM 1= Epiretinal membrane analyzed by HT (first examination), ERM 2= Epiretinal membrane analyzed by HT (second examination), ERM 3= Epiretinal membrane analyzed by ML. 0-ERM not found, 1- ERM found, 2- ERM not assessable. Red= Agreement, Blue=Not Agreement, Purple=Nongradable OCT Image.

		VFT 1				VFT 2				VFT 3			
		Count	0	1	2	Count	0	1	2	Count	0	1	2
VFT 2	0	428	10	15	453	354	7	27	388	357	2	29	388
	Total %	85.60	2.00	3.00	90.60	70.80	1.40	5.40	77.60	71.40	0.40	5.80	77.60
	1	2	3	0	5	0	3	1	4	2	1	1	4
2	0.40	0.60	0.00	1.00	0.00	0.60	0.20	0.80	0.40	0.20	0.20	0.80	
3	13	0	29	42	89	3	16	108	94	2	12	108	
Total %	2.60	0.00	5.80	8.40	17.80	0.60	3.20	21.60	18.80	0.40	2.40	21.60	
4	443	13	44	500	443	13	44	500	453	5	42	500	
Total %	88.60	2.60	8.80		88.60	2.60	8.80		90.60	1.00	8.40		

a- Agreement (HT1-HT2): 92%

b- Agreement (HT1-ML3): 74.6%

c- Agreement (HT2-ML3): 74%

Table 8. Result of Vitreofoveal traction (VFT).

Spectralis OCT findings: VFT1= Vitreofoveolar traction by HT (first examination), VFT 2= Vitreofoveolar traction analyzed by HT (second examination), VFT 3= Vitreofoveolar traction analyzed by ML. 0-VFT not found, 1- VFT found, 2- VFT not assessable. Red= Agreement, Blue=Not Agreement, Purple= Nongradable OCT Image.

		Pseudocyst 1				Pseudocyst 2				Pseudocyst 3			
		Count	0	1	2	Count	0	1	2	Count	0	1	2
Pseudocyst 2	0	200	24	11	235	85	0	9	94	83	2	9	94
	Total %	40.00	4.80	2.20	47.00	17.00	0.00	1.80	18.80	16.60	0.40	1.80	18.80
	1	23	196	4	220	127	149	18	294	125	148	21	294
2	4.60	39.20	0.80	44.60	25.40	29.80	3.60	58.80	25.00	29.60	4.20	58.80	
3	6	7	29	42	17	78	17	112	27	73	12	112	
Total %	1.20	1.40	5.80	8.40	3.40	15.60	3.40	22.40	5.40	14.60	2.40	22.40	
4	229	227	44	500	229	227	44	500	235	223	42	500	
Total %	45.80	45.40	8.80		45.80	45.40	8.80		47.00	44.60	8.40		

a- Agreement (HT1-HT2): 85%

b- Agreement (HT1-ML3): 50.2%

c- Agreement (HT2-ML3): 48.6%

Table 9. Result of Pseudocyst.

Spectralis OCT findings: Pseudocyst 1= Analyzed by HT (first examination), Pseudocyst 2= Analyzed by HT (second examination), Pseudocyst 3=Analyzed by ML. 0- Pseudocyst not found, 1- Pseudocyst found, 2- Pseudocyst not assessable. Red= Agreement, Blue=Not Agreement, Purple= Nongradable OCT Image.

		Splitting 1				Splitting 1				Splitting 2						
		Count	0	1	2	Count	0	1	2	Count	0	1	2			
Splitting 2	0	Count	429	4	15	448	Count	312	1	18	331	Count	311	0	20	331
	0	Total %	85.80	0.80	3.00	89.60	Total %	62.40	0.20	3.60	66.20	Total %	62.20	0.00	4.00	66.20
	1	Count	0	10	0	10	Count	27	13	4	44	Count	31	10	3	44
1	0	Total %	0.00	2.00	0.00	2.00	Total %	5.40	2.60	0.80	8.80	Total %	6.20	2.00	0.60	8.80
2	0	Count	13	0	29	42	Count	103	0	22	125	Count	106	0	19	125
2	1	Total %	2.60	0.00	5.80	8.40	Total %	20.60	0.00	4.40	25.00	Total %	21.20	0.00	3.80	25.00
2	2	Count	442	14	44	500	Count	442	14	44	500	Count	448	10	42	500
2	2	Total %	88.40	2.80	8.80		Total %	88.40	2.80	8.80		Total %	89.60	2.00	8.40	

a- Agreement (HT1-HT2): 93.6%

b- Agreement (HT1-ML3): 69.4%

c- Agreement (HT2-ML3): 68%

Table 10. Result of Splitting.

Spectralis OCT findings: Splitting 1= Analyzed by HT (first examination), Splitting 2= Analyzed by HT (second examination), Splitting 3=Analyzed by ML. 0- Splitting not found, 1- Splitting found, 2- Splitting not assessable. Red= Agreement, Blue=Not Agreement, Purple= Nongradable OCT Image.

		Verticalisation 1				Verticalisation 1				Verticalisation 2						
		Count	0	1	2	Count	0	1	2	Count	0	1	2			
Verticalisation 2	0	Count	407	6	15	428	Count	326	7	25	358	Count	323	7	28	358
	0	Total %	81.40	1.20	3.00	85.60	Total %	65.20	1.40	5.00	71.60	Total %	64.60	1.40	5.60	71.60
	1	Count	9	21	0	30	Count	14	18	3	35	Count	12	21	2	35
1	0	Total %	1.80	4.20	0.00	6.00	Total %	2.80	3.60	0.60	7.00	Total %	2.40	4.20	0.40	7.00
2	0	Count	13	0	29	42	Count	89	2	16	107	Count	93	2	12	107
2	1	Total %	2.60	0.00	5.80	8.40	Total %	17.80	0.40	3.20	21.40	Total %	18.60	0.40	2.40	21.40
2	2	Count	429	27	44	500	Count	429	27	44	500	Count	428	30	42	500
2	2	Total %	85.80	5.40	8.80		Total %	85.80	5.40	8.80		Total %	85.60	6.00	8.40	

a- Agreement (HT1-HT2): 91.4%

b- Agreement (HT1-ML3): 72%

c- Agreement (HT2-ML3): 71.2%

Table 11. Result of Verticalisation.

Spectralis OCT findings: Verticalisation 1= Analyzed by HT (first examination), Verticalisation 2= Analyzed by HT (second examination), Verticalisation 3=Analyzed by ML. 0- Verticalisation not found, 1- Verticalisation found, 2- Verticalisation not assessable. Red= Agreement, Blue=Not Agreement, Purple= Nongradable OCT Image.

		MH 1			MH 1			MH 2					
		Count	0	2	Count	0	2	Count	0	2			
MH 2	0	Count	442	16	458	Count	364	28	392	Count	362	30	392
	0	Total %	88.40	3.20	91.60	Total %	72.80	5.60	78.40	Total %	72.40	6.00	78.40
	1	Count	13	29	42	Count	0	1	1	Count	1	0	1
1	0	Total %	2.60	5.80	8.40	Total %	0.00	0.20	0.20	Total %	0.20	0.00	0.20
2	0	Count	455	45	500	Count	91	16	107	Count	95	12	107
2	1	Total %	91.00	9.00		Total %	18.20	3.20	21.40	Total %	19.00	2.40	21.40
2	2	Count	455	45	500	Count	455	45	500	Count	458	42	500
2	2	Total %	91.00	9.00		Total %	91.00	9.00		Total %	91.60	8.40	

a- Agreement (HT1-HT2): 94.2%

b- Agreement (HT1-ML3): 76%

c- Agreement (HT2-ML3): 74.8%

Table 12. Result of Macular hole (MH).

Spectralis OCT findings: MH1= Macular hole analyzed by HT (first examination), MH2= Macular hole analyzed by HT (second examination), MH3= Macular hole analyzed by ML. 0- Macular hole not found, 1- Macular hole found, 2- Macular hole not assessable. Red= Agreement, Blue=Not Agreement, Purple= Nongradable OCT Image.

		PSM 1						PSM 2			
		Count	0	1	2		Count	0	1	2	
PSM 2	0	408	11	16	434	0 <td>336</td> <td>13</td> <td>27</td> <td>376</td>	336	13	27	376	
	Total %	81.60	2.20	3.00	86.80	0 <td>67.20</td> <td>2.60</td> <td>5.40</td> <td>75.20</td>	67.20	2.60	5.40	75.20	
	1	13	11	0	24	1 <td>9</td> <td>7</td> <td>1</td> <td>17</td>	9	7	1	17	
2	2.60	2.20	0.00	4.80	2 <td>1.80</td> <td>1.40</td> <td>0.20</td> <td>3.40</td>	1.80	1.40	0.20	3.40		
3	13	0	29	42	3 <td>89</td> <td>2</td> <td>16</td> <td>107</td>	89	2	16	107		
Total %	2.60	0.00	5.80	8.40	4 <td>17.80</td> <td>0.40</td> <td>3.20</td> <td>21.40</td>	17.80	0.40	3.20	21.40		
434	22	44	500	5 <td>434</td> <td>22</td> <td>44</td> <td>500</td>	434	22	44	500			
86.80	4.40	8.80	86.80	4.40	86.80	4.40	8.80	86.80			

a- Agreement (HT1-HT2): 89%

b- Agreement (HT1-ML3): 71.8%

c- Agreement (HT2-ML3): 71.8%

Table 13. Result of Pseudomacular hole (PSM).

Spectralis OCT findings: PSM 1= Pseudomacular hole analyzed by HT (first examination), PSM 2= Pseudomacular hole analyzed by HT (second examination), PSM 3= Pseudomacular hole analyzed by ML. 0- Pseudomacular hole not found, 1- Pseudomacular hole found, 2- Pseudomacular hole not assessable. Red= Agreement, Blue=Not Agreement, Purple= Nongradable OCT Image.

		LMH 1						LMH 2			
		Count	0	1	2		Count	0	1	2	
LMH 2	0	427	5	14	446	0 <td>341</td> <td>4</td> <td>29</td> <td>374</td>	341	4	29	374	
	Total %	85.40	1.00	2.80	89.20	0 <td>68.20</td> <td>0.80</td> <td>5.80</td> <td>74.80</td>	68.20	0.80	5.80	74.80	
	1	6	5	1	12	1 <td>10</td> <td>8</td> <td>1</td> <td>19</td>	10	8	1	19	
2	1.20	1.00	0.20	2.40	2 <td>2.00</td> <td>1.60</td> <td>0.20</td> <td>3.80</td>	2.00	1.60	0.20	3.80		
3	13	0	29	42	3 <td>95</td> <td>0</td> <td>12</td> <td>107</td>	95	0	12	107		
Total %	2.60	0.00	5.80	8.40	4 <td>19.00</td> <td>0.00</td> <td>2.40</td> <td>21.40</td>	19.00	0.00	2.40	21.40		
446	10	44	500	5 <td>446</td> <td>10</td> <td>44</td> <td>500</td>	446	10	44	500			
89.20	2.00	8.80	89.20	2.00	89.20	2.00	8.40	89.20			

a- Agreement (HT1-HT2): 92.2%

b- Agreement (HT1-ML3): 73.2%

c- Agreement (HT2-ML3): 72.2%

Table 14. Result of Lamellar macular hole (LMH).

Spectralis OCT findings: LMH 1= Lamellar macular hole analyzed by HT (first examination), LMH 2= Lamellar macular hole analyzed by HT (second examination), LMH 3= Lamellar macular hole analyzed by ML. 0- Lamellar macular hole not found, 1- Lamellar macular hole

found, 2- Lamellar macular hole not assessable. Red= Agreement, Blue=Not Agreement, Purple= Nongradable OCT Image.

		NSD 1				NSD 1				NSD 2			
		0	1	2		0	1	2		0	1	2	
NSD 2	0	321	31	12	364	240	3	15	263	241	9	13	263
	Total %	64.20	6.20	2.40	72.80	48.10	1.60	3.01	52.71	48.30	1.80	2.61	52.71
	1	30	61	3	94	33	67	7	107	35	62	10	107
	Total %	6.00	12.20	0.60	18.80	6.61	13.43	1.40	21.44	7.01	12.42	2.00	21.44
2	3	5	25	42	35	22	22	125	37	23	19	125	
Total %	1.60	1.00	5.00	8.40	17.03	4.41	4.41	25.85	17.43	4.61	3.81	25.85	
3	359	97	44	500	358	97	44	499	363	94	42	499	
Total %	71.80	19.40	8.80		71.74	19.44	8.82		72.75	18.84	8.42		

a- Agreement (HT1-HT2): 82.2% b- Agreement (HT1-ML3): 65.8% c- Agreement (HT2-ML3): 64.4%

Table 15. Result of Neurosensory detachment (NSD). Spectralis OCT findings: NSD 1= Neurosensory detachment analyzed by HT (first examination), NSD 2= Neurosensory detachment analyzed by HT (second examination), NSD 3= Neurosensory detachment analyzed by ML. 0- Neurosensory detachment not found, 1- Neurosensory detachment found, 2- Neurosensory detachment not assessable. Red= Agreement, Blue=Not Agreement, Purple= Nongradable OCT Image.

		PED 1				PED 1				PED 2			
		0	1	2		0	1	2		0	1	2	
PED 2	0	353	14	10	377	249	3	14	266	253	3	10	266
	Total %	70.60	2.80	2.00	75.40	49.80	0.60	2.80	53.20	50.60	0.60	2.00	53.20
	1	11	65	5	81	29	73	10	112	31	67	14	112
	Total %	2.20	13.00	1.00	16.20	5.80	14.60	2.00	22.40	6.20	13.40	2.80	22.40
2	9	4	29	42	95	7	20	122	93	11	18	122	
Total %	1.80	0.80	5.80	8.40	19.00	1.40	4.00	24.40	18.60	2.20	3.60	24.40	
3	373	83	44	500	373	83	44	500	377	81	42	500	
Total %	74.60	16.60	8.80		74.60	16.60	8.80		75.40	16.20	8.40		

a- Agreement (HT1-HT2): 89.4% b- Agreement (HT1-ML3): 68.4% c- Agreement (HT2-ML3): 68.4%

Table 16. Result of Pigment epithelium detachment (PED). Spectralis OCT findings: PED 1= Pigment epithelium detachment analyzed by HT (first examination), PED 2= Pigment epithelium detachment analyzed by HT (second examination), PED 3= Pigment epithelium detachment analyzed by ML. 0- Pigment epithelium detachment not found, 1- Pigment epithelium detachment found, 2- Pigment epithelium detachment not assessable. Red= Agreement, Blue=Not Agreement, Purple= Nongradable OCT Image.

		ELM 1				ELM 1				ELM 2			
		Count	0	1	2	Count	0	1	2	Count	0	1	2
ELM2	0	231	72	10	313	122	11	7	140	129	6	5	140
	1	46.20	14.40	2.00	62.60	24.40	2.20	1.40	28.00	25.60	1.20	1.00	28.00
	2	21	115	5	141	84	59	12	155	103	67	15	185
		4.20	23.60	1.00	29.00	16.80	17.60	2.40	37.00	20.60	13.40	3.00	37.00
		6	7	25	42	52	38	25	115	81	72	22	175
		1.20	1.40	5.00	8.40	10.40	19.60	5.00	35.00	16.20	14.40	4.40	35.00
		258	198	44	500	258	198	44	500	313	145	42	500
		51.60	39.60	8.80		51.60	39.60	8.80		62.60	29.00	8.40	

a- Agreement (HT1-HT2): 75.8%

b- Agreement (HT1-ML3): 47.2%

c- Agreement (HT2-ML3): 43.6%

Table 17. Result of External limiting membrane (ELM).

Spectralis OCT findings: ELM 1= External limiting membrane analyzed by HT (first examination), ELM 2= External limiting membrane analyzed by HT (second examination), ELM 3= External limiting membrane analyzed by ML. 0- ELM was normal, 1- ELM was abnormal, 2- ELM was not assessable. Red= Agreement, Blue=Not Agreement, Purple= Nongradable OCT Image.

		IS/OS 1				IS/OS 1				IS/OS 2			
		Count	0	1	2	Count	0	1	2	Count	0	1	2
IS/OS 2	0	185	77	6	268	103	11	7	121	114	3	4	121
	1	37.00	15.40	1.20	53.60	20.60	2.20	1.40	24.20	22.80	0.60	0.80	24.20
	2	13	168	9	190	53	136	12	206	85	105	16	206
		2.60	33.60	1.80	38.00	11.60	27.20	2.40	41.20	17.00	21.00	3.20	41.20
		3	10	29	42	40	108	25	173	65	82	22	173
		0.60	2.00	5.80	8.40	8.00	21.60	5.00	34.60	13.80	16.40	4.40	34.60
		201	255	44	500	201	255	44	500	268	190	42	500
		40.20	51.00	8.80		40.20	51.00	8.80		53.60	38.00	8.40	

a- Agreement (HT1-HT2): 76.4%

b- Agreement (HT1-ML3): 52.8%

c- Agreement (HT2-ML3): 48.2%

Table 18. Result of Photoreceptors inner and outer segments (IS/OS).

Spectralis OCT findings: IS/OS 1= Photoreceptors inner and outer segments analyzed by HT (first examination), IS/OS 2= Photoreceptors inner and outer segments analyzed by HT (second examination), IS/OS 3= Photoreceptors inner and outer segments analyzed by ML. 0- IS/OS was normal, 1- IS/OS was abnormal, 2- IS/OS was not assessable. Red= Agreement, Blue=Not agreement, Purple= Nongradable OCT image.

3.7 Total results of morphological findings

When analyzing the variables we found that the degree of agreement between HT1 and HT2 is above 379/500 (75.8%) of the images valued in ELM and up to 471/500 (94.2%) in MH. In the analysis between HT1 and ML3, the greater percentage of agreement occurred between images in patients with MH by 380 (76%) while the lowest agreement was observed in the images of ERM with 226/500 (45.2%), obtaining a 37% decrease compared to HT1 and HT2 analysis.

When analyzing the degree of agreement between HT2 and ML3, we found that the greatest degree of agreement was observed also in MH, with 374/500 (74.8%), while in ERM the results obtained were very low with only 193/500 (38.6%).

Therefore, a decrease was observed in the degree of intraobserver agreement from 86.30% to 63.21% and 61.66% of the interobserver (**Table 19**).

VARIABLES	HT1-HT2		HT1-ML3		HT2-ML3	
	N	(%)	N	(%)	n	(%)
FO_DE	392	(78.4)	277	(55.2)	299	(57.8)
ERM	411	(82.2)	226	(45.2)	193	(38.6)
VFT	460	(92)	373	(74.6)	370	(74)
Pseudocyst	425	(85)	251	(50.2)	243	(48.6)
Splitting	468	(93.6)	347	(69.4)	340	(68)
Verticalisation	457	(91.4)	360	(72)	356	(71.2)
MH	471	(94.2)	380	(76)	374	(74.8)
PSM	448	(89.6)	359	(71.8)	359	(71.8)
LMH	461	(92.2)	366	(73.2)	361	(72.2)
NSD	411	(82.2)	329	(65.8)	322	(64.4)
PED	447	(89.4)	342	(68.4)	342	(68.4)
ELM	379	(75.8)	236	(47.2)	218	(43.6)
IS/OS	382	(76.4)	264	(52.8)	241	(48.2)
TOTAL		86.30%		63.21%		61.66%

Table 19. Degree of agreement in morphological findings.

Percentage of variables with greater agreement in 500 patients with macular diseases. HT1= First exploration by HT, HT2=Second exploration by HT, ML3=First examination by ML. MH=Macular hole, LMH=Lamellar macular hole, VFT=Vitreofoveolar traction, PSM=Pseudomacular hole, PED=Pigment epithelium detachment, NSD=Neurosensory detachment, ERM=Epiretinal membrane, Fo_De=Foveal depression, IS/OS=Photoreceptors inner and outer segments, ELM=External limiting membrane.

3.8 Results of nongradable morphological findings

Percentages of nongradable is used to display which is the most difficult morphological finding to detect an image of Spectralis OCT. ELM was the feature most discarded with 175/500 (35%) by ML3, while MH and foveal depression was the variable most excluded by HT with 45/500 (9%) respectively. Also we can observe that images not valued (nongradable) among the first scan and the second scan were very identical, between 8 and 9% by HT whereas by ML3 had an increment more than 15% in all of them.

Therefore, we found that the retina specialist ruled out a greater number of images 24.52% than general ophthalmologist 8.83% (**Table 20**).

Variables	HT1		HT2		ML3	
	N	(%)	N	(%)	n	(%)
FoDe	45	(9)	42	(8.4)	108	(21.6)
ERM	44	(8.8)	42	(8.4)	114	(22.8)
VFT	44	(8.8)	42	(8.4)	108	(21.6)
Pseudocyst	44	(8.8)	42	(8.4)	112	(22.4)
Splitting	44	(8.8)	42	(8.4)	125	(25)
Verticalisation	44	(8.8)	42	(8.4)	107	(21.4)
MH	45	(9)	42	(8.4)	107	(21.4)
PSM	44	(8.8)	42	(8.4)	107	(21.4)
LMH	44	(8.8)	42	(8.4)	107	(21.4)
NSD	44	(8.8)	42	(8.4)	129	(25.8)
PED	44	(8.8)	42	(8.4)	122	(24.4)
ELM	44	(8.8)	42	(8.4)	175	(35)
IS/OS	44	(8.8)	42	(8.4)	173	(34.6)
Total		8.83 %		8.40 %		24.52 %

Table 20. Nongradable morphological findings.

Percentage of variables more images not valued in 500 patients with macular diseases. HT1= First exploration by HT, HT2=Second exploration by HT, ML3=First exploration by ML. MH=Macular hole, LMH=Lamellar macular hole, VFT=Vitreofoveal traction, PSM=Pseudomacular hole, PED=Pigment epithelium detachment, NSD=Neurosensory detachment, ERM=Epiretinal membrane, Fo_De=Foveal depression, IS/OS=Photoreceptors inner and outer segments, ELM=External limiting membrane, n= Number of patients.

4. Discussion

In the last decade, OCT has emerged as a useful and adjunctive imaging technique, providing high-resolution cross-sectional images and valuable information about various pathologic features of the macula (Huang D, Swanson EA, Lin CP et al. 1991; Puliafito CA, Hee MR, Lin CP et al.1995). Quantification of macular thickness by OCT in a reproducible, non-invasive way allows clinicians to monitor the efficacy of treatment for macular pathologic features like diabetic macular edema (Lam DS, Chan CK, et al. 2007; Chew E, Strauber S, et al. 2007).

Spectral-domain OCT has revolutionized the diagnostic and examination in a number of vitreoretinal conditions like macular edema (ME) associated with vascular occlusions, diabetic retinopathy, ARMD and vitreoretinal interface disorders. (Forooghian F, et al 2008; Yamaike N, et al. 2008; Fleckenstein M, et al. 2008). Also provides a higher sensitivity to detect morphological changes that occur in the preretinal, intraretinal, subretinal and sub/RPE space; such as ERM, macular holes, accumulation of intraretinal fluid, pigment epithelium detachment and photoreceptor outer segment disruption (Keane PA, Bhatti RA, 2009).

However, even though the revolutionary improvement in the imaging of the eye, some difficulties become evident in the evaluating the obtained OCT images, The new spectral-domain OCT device provides special software showing the segmentation of the retinal layers. Consequently those positions are regulated automatically by the software of each instrument (Wolf-Schnurrbusch UE, Ceklic L, et al., 2009). The identification of the artifacts of the images and falsely settled segmentation lines are important to avoid the errors created by the OCT devices (Ian C, Han, MD, Glenn J. Jaffe, MD, 2010).

The second method for analyzing the OCT images is the manual measurement, where the observer marks, with the caliper, the areas of interest by using the software provided by the OCT-machine. Even though overcoming the segmentation errors created by the OCT-machine, subjectivity of this method is the major limitation (Wolf-Schnurrbusch UE, Ceklic L, et al., 2009).

Our study was designed to analyze the concordance between a general ophthalmologist and a retina specialist in the interpretation of Spectralis OCT images obtained in five of the most common macular diseases ARMD, BRVO, CRVO, DME and ERM.

According to the intraobserver analysis obtained by the general ophthalmologist in two examinations (HT1-HT2), in each group of macular diseases the mean difference of CRT was not found to be statistically significant (**Table 3**).

In the first interobserver analysis (HT1-ML3) of the CRT, a high degree of agreement in ARMD and CRVO was seen. ARMD was the disease with the lowest mean CRT (230.99 μ m by HT1 and 232.87 μ m by ML3) while CRVO showed the highest mean CRT with (598.22 μ m by HT1 and 586.74 μ m by ML3). In contrast, other diseases such as BRVO (347.97 μ m by HT1 and 321.78 μ m by ML3), DME (408.38 μ m by HT1 and 393.56 μ m by ML3) and ERM (293.24 μ m by HT1 and 260.97 μ m by ML3), the disagreement was statistically significant (BRVO: P=0.004, DME: P=0.02, ERM: P=0.0007 (**Table 4**).

A possible explanation for these discrepancies could be the negative transfer of experience from the TD-OCT by the general ophthalmologist, since the inferior limit of the CRT measurements were tended to end (**Fig. 34**), at the IS/OS junction whereas the retina specialist included the outer boundary of RPE/Bruch membrane complex in the measurement by using the TD-OCT (**Fig. 35**). The general ophthalmologist measured from the internal

limiting membrane (ILM) and the junction of the outer and inner segment of the photoreceptors (IS/OS) whereas the retina specialist measured from the outer boundary includes the RPE/Bruch membrane complex.

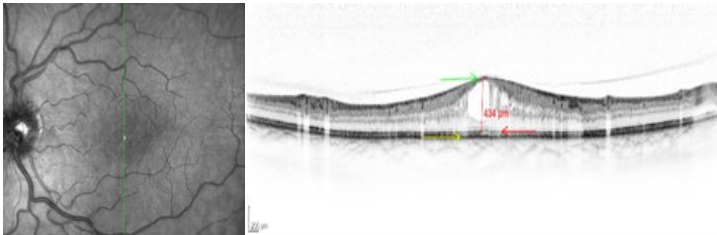


Fig. 34: Spectralis OCT vertical line scan shows CRT measurement of 434 μm from ILM (green arrow) to the junction of the IS/OS (red arrow) by the general ophthalmologist.

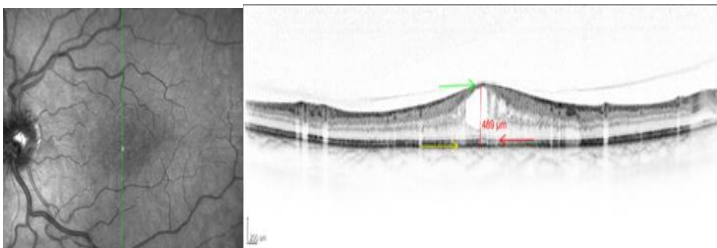


Fig. 35: Spectralis OCT vertical line scan shows the correct CRT measurement (489 μm) from ILM (green arrow) to RPE/Bruch membrane complex (yellow arrow) by the retina specialist.

Previous studies have reported that SD-OCT and TD-OCT have a significant difference in measuring the boundaries of CRT (Han IC, Jaffe G, 2008; Grover S et al. 2009; Giani A et al. 2010; Piero L et al. 2010). TD-OCT

generated segmentation system uses the IS/OS hyper-reflective band for boundary in the measurement of the CRT. The new SD-OCT system is capable to show in the outer retinal layers three distinct hyper-reflective bands. The bands correspond to the ELM, IS/OS and the RPE.

The SOCT Copernicus, Spectral OCT/SLO, RTvue-100 and 3D OCT-1000 use the second inner hyper-reflective band as the outer border of the retina. Cirrus HD-OCT and Spectralis HRA+OCT identify the external reflective band as the outer border RPE/Bruch's membrane complex if automatically generated segmentation protocol is chosen. (Wolf-Schnurrbusch UE, Ceklic L, et al., 2009).

In the second interobserver analysis (HT2-ML3) of the mean CRT considering all the five diseases, the mean difference of the CRT ranged from (4.66 to 29.20 μm); the disagreement was a statistically significant in BRVO ($P < 0.03$) and ERM ($P < 0.02$) but not for ARMD, CRVO and DME. The CRT measurements in ARMD, CRVO and DME were within the agreement limits. However in BRVO ($P < 0.03$) and ERM ($P < 0.02$) statistically significant interobserver disagreement was found. These results can be interpreted as a positive effect of the learning curve of the general ophthalmologist in the second analysis (**Table 5**).

The intra- and interobserver agreement in identifying the predetermined morphological findings in the macula was analyzed, which are seen in the selected five different diseases. Of the 13 morphological findings, the average agreement for detection of all features in this study was 86.30% for HT1 vs HT2 (intraobserver), 63.21% for HT1 vs. ML (interobserver 1) and 61.66% for HT2 vs ML (interobserver 2).

We note that the highest degree of agreement between the two observers was in the intraretinal layers (MH, LMH, PSM, verticalisation, splitting); MH was the feature with the highest degree of agreement of 78.4%, while the lowest degree of agreement was ERM in the preretinal space with 38.6%, followed by subretinal features ELM and IS /OS with 43.6% and 48.2% respectively (**Table 19**).

According to Keane PA and associates, SD-OCT has a high sensitivity and high resolution to distinguish and detect relevant morphological changes in the preretinal space (e.g. ERM and VMT) as well as MH and fine structures of the subretinal space (Keane PA et al., 2009). Also Knecht PB and associates, have mentioned that the Spectralis OCT had a good degree of agreement between observers to detect ERM and pseudocyst and a low level of agreement for detecting subretinal

morphological changes as ELM and IS/ OS (Knecht PB et al., 2013).

In our study, we found that besides the high sensitivity and high resolution imaging by Spectralis OCT in detecting macular morphological findings, the interpretation of the findings were not free of bias, based mainly on the learning curve. Consequently, the therapy decisions may therefore show considerable differences in some eyes based on the experience of the observer.

By analyzing the nongradable OCT-images of the morphological findings, we observed no significant difference in all the variables by the general ophthalmologist (HT1: 8.83%, HT2: 8.4%) (**Table 20**). In comparison with the retina specialist for the gradability revealed a significant disagreement in all the variables ML3: 24.52%. ELM: 35% and IS/OS: 34.6% the variables most discarded were by the retina specialist (**Fig. 36**).

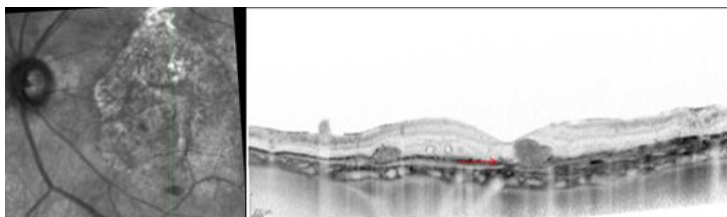


Fig. 36: Spectralis OCT vertical line scan shows an insufficient image quality of the macula for distinguish ELM and IS/OS (red arrow). This

image was decided as nongradable by the retina specialist. Note the poor saturation of the image.

The detection of the ELM and IS/OS can offer difficulties, if the macular morphology is presented with additional changes in the pigment epithelium (Knecht PB et al., 2013). It was also mentioned that thanks to the high resolution of SD-OCT, in general, it is easier to detect morphological changes in preretinal and subretinal spaces than within the retina. Therefore, our results were probably due to the learning curve of the general ophthalmologist.

The recent advances in the treatment of the frequently seen macular diseases, such as ARMD, BRVO, CRVO, DME and ERM lead to a considerable increase in the number of patients, with the need of active follow-up examinations in relatively short intervals. Currently, before any clinical decision for a treatment of a macular disease, an OCT examination is *qua sine none*. Even though the Spectralis OCT is a very useful tool in distinguishing and detecting morphological findings in various macular diseases, the captured images needs to be interpreted correctly. Our analysis was aimed to find the general agreement between a general ophthalmologist without any experience in interpreting the Spectralis OCT and a

retina specialist, trained in Spectralis OCT. For this analysis we chose five most common retinal diseases with macular affection. We found considerable interobserver disagreement in the decision for the gradability of the OCT images. We also observed a tendency for improved interpretation of the general ophthalmologist in the second analysis. For the ARMD, CRVO and DME the interobserver agreement was in concordance (ARMD: 228.18 μm by HT2 and 232.87 μm by ML3, $P= 0.36$; CRVO: 591.40 μm by HT2 and 586.74 μm by ML3, $P= 0.55$; and DME: 406.70 μm by HT2 and 393.56 μm by ML3, $P= 0.08$). However for some findings, such as (BRVO: 338.40 μm by HT2 and 321.78 μm by ML3, $P= 0.03$; ERM: 290.17 μm by HT2 and 260.97 μm by ML3, $P= 0.02$) the decision made by the general ophthalmologist was not sufficient (disagreement statistical significant) **(Table 5)**.

In summary, in the fellowship period of the posterior segment diseases, the education program or inexperienced ophthalmologists should consider an intensive teaching period in interpreting OCT examinations.

5. Summary

The macula is the center of the posterior pole, and responsible for high acuity vision which is important for facilities like reading, writing, driving and working on the computer. Macular edema (ME) is the most common pathology of the macula resulting in impairment of central vision. Diseases such as diabetic macular edema (DME), age-related macular degeneration (ARMD), retinal vascular occlusive diseases, and vitreoretinal interface disorders are the most frequent reasons of ME. Developments in pharmacotherapy provide effective treatment options for some macular diseases. ME presents with morphological findings in the preretinal, intraretinal and subretinal space. It is also associated with changes in the retinal pigment epithelium and choriocapillaris complex.

Recent technological advances in the optical coherence tomography (OCT) have resulted in high-resolution imaging of the macula and their morphological changes. Spectralis OCT has a scan speed of 40,000 A-scans per second with 7 μ m optical and 3.9 μ m digital axial resolution and is an effective tool in the detection, evaluation and monitoring of the central retinal thickness

measurement (CRT) and morphological retinal features in vitreoretinal disorders.

It also became evident, that despite the improvement of the OCT-techniques, the measurements and interpretation of the macular morphology may vary according to several factors such as the type of the OCT machine, the quality of the captured images, the experience of the physician and lastly the complexity of the findings.

Therefore we aimed to analyze the agreement between a general ophthalmologist (intraobserver) and a specialist of the retinal diseases (interobserver) in the OCT-examination of different macular diseases. The examination included the measurement of the CRT and the identification of morphological findings in 500 eyes of 500 patients. In total, 100 eyes of five different diseases (AMD, diabetic macular edema, branch retinal vein occlusion, central retinal vein occlusion and epiretinal membrane) were selected.

The comparison between the first and second CRT-measurement by the general ophthalmologist (intraobserver agreement) were statistically not significant. In other words, the CRT-measurements of the general ophthalmologist in the two consecutive sessions did not reveal a meaningful

difference considering the whole eyes and each separate disease.

In the first interobserver analysis, the CRT-measurements were in concordance in eyes having ARMD ($P=0.84$) and CRVO ($P=0.35$). In eyes with DME ($P<0.02$), BRVO ($P<0.004$) and ERM ($P<0.0007$), the comparison of the CRT-measurements showed a poor agreement.

The second interobserver analysis for the CRT-measurements revealed a general improvement of the general ophthalmologists. In three diseases, ARMD ($P=0.36$), CRVO ($P=0.55$), and DME ($P=0.08$), the comparison did not show a statistical significance. The comparison in BRVO ($P<0.03$) and ERM ($P<0.02$) revealed a statistical significance between the measurement of the observers.

In the analysis of the predetermined morphological findings, the highest agreement between the two observers was the identification of the features within the retinal layers, such as MH, LMH, PSM, verticalisation and splitting; MH was the feature with the highest agreement with 78.4%. Interestingly, the lowest agreement was ERM in the preretinal space with 38.6%, followed by subretinal features ELM and IS /OS with 43.6% and 48.2% respectively.

In summary, we found intraobserver and interobserver differences exist in analysis of the images taken by the Spectralis-OCT in several macular diseases. A training course of three months for the general ophthalmologist has resulted in improved interpretation of some morphological features in macula. However, based on the result of our study, a longer period with an intensive, interactive teaching program is needed for a general ophthalmologist for a reliable analysis of Spectralis-OCT images in macular diseases.

6. Bibliography

Alam S, Zawadzki RJ, Choi S, et al.

Clinical application of rapid serial Fourier-domain optical coherence tomography for macular imaging.

Ophthalmology 2006; 113: 1425-1431

Altman DG, Bland JM

Measurement in medicine: the analysis of method comparison studies.

The Statistician 1983; 32: 307–317

American Academy of Ophthalmology. The eye
M.D. Association

Retina and Vitreous

Basic and Clinical Science Course

Leo, copyright © 2011; Section 12: 8-17

Appiah AP, Hirose T

Secondary causes of premacular fibrosis.

Ophthalmology 1989; 96: 389-392

Arevalo JF et al.

Primary intravitreal bevacizumab for subfoveal choroidal neovascularization in Age-Related Macular Degeneration.

Retina 2008; (10) 1387-1394

Bakall B, Folk JC, Boldt HC, Sohn E, et al.

Aflibercept therapy for exudative age-related macular degeneration resistant to bevacizumab and ranibizumab.

Am J Ophthalmology 2013; 156: 15-22

Bandello F, Battaglia Parodi M, Schmidt-Erfurth U et al.

Anti-VEGF; Anti-VEGF Factors in Age-Related Macular Degeneration

Dev Ophthalmology. Basel, Karger, 2010; vol. 46: 21-38

Bandello F, Battaglia Parodi M, Siemerink MJ et al.

Anti-VEGF; Mechanisms of ocular Angiogenesis and its molecular mediators

Dev Ophthalmology. Basel, Karger, 2010; vol. 46:
4-20

Bearely S, Chau FY, Koreishi A, et al.

Spectral domain optical coherence tomography
imaging of geographic atrophy margins.

Ophthalmology 2009; 116: 1762-1769

Bland JM, Altman DG

Statistical methods for assessing agreement
between two methods of clinical measurement.

Lancet 1986; 327: 307–10

Brooks HL Jr

Macular hole surgery with and without internal
limiting membrane peeling.

Ophthalmology 2000; 107: 1939-1948

Chen TC, Cense B, Pierce MC, et al.

Spectral domain optical coherence tomography: ultrahigh, speed, ultrahigh resolution ophthalmic imaging.

Arch Ophthalmol 2005; 123: 1715-1720

Catier A, Tadayoni R, Paques M et al.

Characterization of macular edema from various etiologies by optical coherence tomography.

Am J Ophthalmology 2005; 140: 200-206

Chang LK, Fine HF, Spaide RF, et al.

Ultrastructural correlation of spectral-domain optical coherence tomographic findings in vitreomacular traction syndrome.

Am J Ophthalmology 2008; 146: 121-127

Chew E, Strauber S, Beck R, et al.

Diabetic Retinopathy Clinical Research Network. Randomized trial of peribulbar triamcinolone acetonide with and without focal photocoagulation for mild diabetic macular edema: a pilot study.

Ophthalmology 2007; 114: 1190-1196

Coscas G, et al.

Optical Coherence Tomography in Age-Related Macular Degeneration

Springer Medizin Verlag Heidelberg 2009; 20

Costa RA, Calucci D, Skaf M et al

Optical coherence tomography 3: automatic delineation of the outer neural retinal boundary and its influence on retinal thickness measurements.

Invest Ophthalmology Vis Sci 2004; 45: 2399-2406

Drexler W, Fujimoto JG.

State of the art retinal optical coherence tomography.

Retina Eye Res 2008; 27: 45-88

Drexler W, Sattmann H, Hermann B, et al.

Enhanced visualization of macular pathology with the use of ultrahigh resolution optical coherence tomography.

Arch Ophthalmology 2003; 121: 695-706

Duker JS, Brown GL

Anterior location of the crossing artery in branch retinal vein occlusion.

Arch Ophthalmology 1989; 107: 998-1000

Elman MJ, Bressler NM, Qin H, et al.

Expanded 2-year follow-up of ranibizumab plus prompt or deferred laser or triamcinolone plus prompt laser for diabetic macular edema.

Ophthalmology 2011; 118: 609-614

ETDRS Research Group (1991)

Early photocoagulation for diabetic retinopathy.

ETDRS Report Number 9. Ophthalmology 98 (suppl):766-785

ETDRS Research Group (1991)

Fundus photographic risk factors for progression of diabetic retinopathy.

ETDRS Report Number 12. Ophthalmology 98 (Suppl): 823-833

ETDRS Research Group (1991)

Grading diabetic retinopathy from stereoscopic color fundus photographs-an extension of the modified Airlie house classification.

ETDRS Report Number 10. Ophthalmology 98 (Suppl): 786-805

Fercher F, C. K. Hitzenberger, W. Drexler, G. Kamp, and H. Sattmann.

In Vivo Optical Coherence Tomography.

Am. J. Ophthalmology 1993; vol. 116, no. 1, pp. 113-114

Fercher AF, Hitzenberger CK, Kamp G, Elzaiat SY.

Measurement of intraocular distances by backscattering spectral interferometry.

Opt Commun 1995; 117: 43-48

Fleckenstein M, Charbel Issa P, Helb HM, et al.

High-resolution spectral domain-OCT imaging in geographic atrophy associated with age-related macular degeneration.

Invest Ophthalmology Vis Sci 2008; 49: 4137-4144

Forooghian F, Cukras C, Meyerle CB, et al.

Evaluation of time domain and spectral-domain optical coherence tomography in the measurement of diabetic macular edema.

Invest Ophthalmol Vis Sci 2008; 49: 4290-4296

Gass JD.

Reappraisal of biomicroscopic classification of stages of development of a macular hole.

Am J Ophthalmology; 1995; 119: 752–759.

Gass JD, Joondeph BC.

Observations concerning patients with suspected impending macular holes.

Am J Ophthalmology 1990; 109: 638–646.

Giani A, Cigada M, Staurenghi G et al.

Reproducibility of Retinal Thickness Measurements on Normal and Pathologic Eyes by Different Optical Coherence Tomography Instruments.

Am J Ophthalmol 2010; 150:815-824

Green WR

Histopathology of age-related macular degeneration.

Mol Vis. 1999; 5: 27

Grover S, Murthy RK, Brar VS, Chalam KV.

Normative data for macular thickness by high-definition spectral-domain optical coherence tomography (Spectralis).

Am J Ophthalmol 2009; 148 :266-271

Gupta V, Gupta A, Dogra M

Atlas Optical coherence tomography of macular diseases

Jaypee 2004; 18-20

Haller JA, Qin H, Apte RS, et al.

Vitrectomy outcomes in eyes with diabetic macular edema and vitreomacular traction.

Ophthalmology 2010; 117: 1087-1093

Han IC, Jaffe GJ

Comparison of spectral-and time-domain optical coherence tomography for retinal thickness measurements in healthy and diseased eyes.

Am Ophthalmol 2009; 147: 847-858, 858 e 841

Han IC, Jaffe GJ

Evaluation of Artifacts Associated with macular Spectral-Domain OCT

Ophthalmology 2010; 117: 1177-1189

Hayreh SS

Classification of central retinal vein occlusion.

Ophthalmology. 1983; 90: 458-474

Hayreh SS, Zimmerman M.B., Podhajsky P

Incidence of various types of retinal vein occlusion and their recurrence and demographic characteristics.

Am J Ophthalmology. 1994; 117: 429-441

Hee MR, Izatt JA, Swanson EA et al.

Optical coherence tomography of the human retina.

Arch Ophthalmol 1995; 113: 325-332.

Hee MR, Puliafito CA, Wong C, et al.

Optical coherence tomography of macular holes.

Ophthalmology 1995; 102: 748–756

Hee MR, Puliafito CA, Wong C, et al.

Quantitative assessment of macular edema with optical coherence tomography.

Arch Ophthalmology 1995; 113: 1019–1029

Hirvela H, Luukinen H, Laara E, et al.

Risk factors of age-related maculopathy in a population 70 years of age or older.

Ophthalmology 1996; 103: 871-877

Holash J, Davis S, Papadopoulos N, et al.

VEGF-Trap: a VEGF blocker with potent antitumor effects.

Proc Natl Acad Sci USA 2002; 99: 11393-11398

Huang D, Swanson EA, Lin CP et al.

Optical coherence tomography.

Science 1991; 254: 1178-1181.

Ian C, Han MD, Jaffe GJ, MD

Evaluation of artifacts associated with macular spectral-domain optical coherence tomography.

Ophthalmology 2010; 117: 1177-1189

Jansz P, Richardson S, Wild G, Hinckley S

Biomedical Image Signal Processing for Reflection-Based Imaging

Intech science 2012; 16: 362

Johnson MW

Perifoveal vitreous detachment and its macular complications.

Am Ophthalmology Soc. 2005; 103: 537-567

Johnson MW

Tractional cystoid macular edema: a subtle variant of the vitreomacular traction syndrome.

Am J Ophthalmology. 2005; 140: 184-192

Keane PA, Bhatti RA, Brubaker JW et al.

Comparison of clinically relevant findings from High-Speed Fourier-Domain and Conventional Time-Domain optical coherence tomography.

Am J Ophthalmol 2009; 148: 242-248

Kelly NE, Wendel RT

Vitreous surgery for idiopathic macular holes. Results of a pilot study.

Arch Ophthalmology. 1991; 109: 654-659

Kim NR, Kim YJ, Chin HS, et al.

Optical coherence tomographic patterns in diabetic macular edema: prediction of visual outcome after focal laser photocoagulation.

Br J Ophthalmology. 2009; 93: 901-905

Klein R, Moss SE, Klein BEK, Davis MD, DeMets DL.

The Wisconsin epidemiologic study of diabetic retinopathy. XI. The incidence of macular edema.

Ophthalmology 1989; 96:1501–1510

Knecht PB, Kordic H, Kurz-Levin M, Sturm V, Menke MN.

Inter-observer agreement for spectral- and time-domain optical coherence image grading: a prospective study.

Int Ophthalmol 2013; 33: 47-52

Lam DS, Chan CK, Mohamed S, et al.

Intravitreal triamcinolone plus sequential grid laser versus triamcinolone or laser alone for treating diabetic macular edema. Six months outcomes.

Ophthalmology 2007; 114: 2162-2167

Leitgeb RA, Drexler W, Unterhuber A, et al.

Ultrahigh resolution Fourier domain optical coherence tomography.

Opt Express 2004; 12: 2156–2165

Lerche RC, Schaudig U, Scholz F et al.

Structural changes of the retina in retinal vein occlusion: imaging and quantification with optical coherence tomography.

Ophthalmic Surg Lasers 2001; 32: 272-280

Martin DF et al.

Ranibizumab and Bevacizumab for treatment of neovascular Age-Related Macular Degeneration.

Ophthalmology 2012; 119 (7) 1338-1398

Massin P, Duguid G, Erguinay A, Haouchine B, Gaudric A.

Optical coherence tomography for evaluating diabetic macular edema before and after vitrectomy.

Am J Ophthalmology 2003; 135 (2):169-177

Massin P, Erguinay A, Haouchine B, Mehidi AB, Paques M, Gaudric A

Retinal thickness in healthy and diabetic subjects measured using optical coherence tomography mapping software.

Eu J Ophthalmology 2002; 12 (2):102-108

McCarty DJ, Mukesh BN, Chikani V, et al.

Prevalence and associations of epiretinal membranes in the visual impairment project.

Am J Ophthalmology. 2005; 140: 288-294

Menke MN, Dabov S, Knecht P, Sturm V

Reproducibility of retinal thickness measurements in healthy subjects using Spectralis optical coherence tomography.

Am J Ophthalmology 2009; 147: 467-472

Michaelides M, Kaines A, Hamilton RD, et al.

A prospective randomized trial of intravitreal bevacizumab or laser therapy in the management of diabetic macular edema (BOLT study) 12-month data report 2.

Ophthalmology. 2010; 117: 1078-1086

Nassif NA, Cense B, Park BH, et al.

In vivo high-resolution video-rate spectral-domain optical coherence tomography of the human retina and optic nerve.

Opt Express 2004; 12: 367–376

Nussenblat RB, Kaufman SC, Palestine AG, Davis MD, Ferris FL.

Macular thickening and visual acuity.

Ophthalmology. 1987; 94: 1134–1139

Ota M, Tsujikawa A, Murakami T, et al.

Foveal photoreceptor layer in eyes with persistent cystoid macular edema associated with branch retinal vein occlusion.

Am J Ophthalmology. 2008; 145: 273-280

Otani T, Kishi S, Maruyama Y

Patterns of diabetic macular edema with optical coherence tomography.

Am J Ophthalmology. 1999; 127: 688-693

Ozdemir H, Karacorlu M., Karacorlu S

Serous macular detachment in central retinal vein occlusion.

Retina 2005; 25: 561-563

Pierro L, Giatsidis SM, Mantovani E, Gagliardi M.

Macular thickness Interoperator and Intraoperator Reproducibility in healthy Eyes Using 7 Optical Coherence Tomography instruments

Am J Ophthalmol 2010; 150: 199-204

Pons ME, García-Valenzuela E

Redefining the limit of the outer retina in optical coherence tomography scans.

Ophthalmology 2005; 112: 1079-1085

Puliafito CA, Hee MR, Lin CP et al.

Imaging of macular diseases with optical coherence tomography.

Ophthalmology 1995; 102: 217-229

Ray R, Stinnet SS, Jaffe GJ.

Evaluation of image artifact produced by optical coherence tomography of retinal pathology.

Am J Ophthalmology; 2005; 139:18-29

Roquet W, Roudot-Thoraval F, Coscas G, et al.

Clinical features of drusenoid pigment epithelial detachment in age related macular degeneration.

Br J Ophthalmology 2004; 88: 638-642

Ryan S, Schachat A, Wilkinson C, Hinton D, Sadda S, Wiedemann P

Retina

Elsevier 5th Edition 2013; Part 1, section 1

Sadda SR, Joeres S, Wu Z et al.

Error correction and quantitative subanalysis of optical coherence tomography data using computer-assisted grading.

Invest Ophthalmology Vis Science 2007; 48: 839-848

Sadda SR, Wu Z, Walsh AC et al.

Errors in retinal thickness measurements obtained by optical coherence tomography.

Ophthalmology 2006; 113: 285-293

Schmidt-Erfurth U, Leitgeb RA, Michels S, et al.

Three-dimensional ultra-high resolution optical coherence tomography of macular diseases.

Invest Ophthalmol Vis Sci 2005; 46: 3393-3402

Schuman JS, Puliafito CA

Optical coherence tomography of ocular diseases.

Slack Thorofare, NJ 2004

Shroff D, Mehta DK, Arora R, et al.

Natural history of macular status in recent-onset branch retinal vein occlusion: an optical coherence tomography study.

Int Ophthalmology. 2008; 28: 261-268

Sikorski BL, Bukowska D, Kaluzny JJ, et al.

Drusen with accompanying fluid underneath the sensory retina.

Ophthalmology 2010; 118: 82-92

Smiddy WE, Maguire AM, Green WR, et al.

Idiopathic epiretinal membranes. Ultrastructural characteristics and clinic pathologic correlation.

Ophthalmology 1989; 96: 811-820

Smiddy WE, Michels RG, Green WR

Morphology, pathology, and surgery of idiopathic vitreoretinal macular disorders.

Retina 1990; 10: 288-296

Soliman W, Sander B, Hasler PW, et al.

Correlation between intraretinal changes in diabetic macular edema seen in fluorescein angiography and optical coherence tomography.

Acta Ophthalmology 2008; 86: 34-39

Soliman W, Sander B, Soliman KA, et al.

The predictive value of optical coherence tomography after grid laser photocoagulation for diffuse diabetic macular edema.

Acta Ophthalmology 2008; 86: 284-291

Spaide RF, Curcio CA

Drusen characterization with multimodal imaging.

Retina 2010; 30: 1441-1454

Spaide RF, Curcio CA

Anatomical correlates to the bands seen in the outer retina by OCT.

Retina 2011; 31:1609-1619

Srinivasan VJ, Monson BK, Wojtkowski M, et al.

Characterization of outer retinal morphology with high-speed, ultrahigh-resolution optical coherence tomography.

Invest Ophthalmology Vis Sci. 2008; 49: 1571-1579

Srinivasan VJ, Wojtkowski M, Witkin AJ et al.

High-definition and three-dimensional imaging of macular pathologies with high-speed ultrahigh-resolution optical coherence tomography.

Ophthalmology 2006; 113: 2054-2065

Srinivasan VJ, Ko TH, Wojtkowski M, et al.

Noninvasive volumetric imaging and morphometry of the rodent retina with high-speed, ultrahigh-resolution optical coherence tomography.

Invest Ophthalmology Vis Sci. 2006; 47: 5522-5528

Stewart MW, Rosenfeld PJ

Predicted biological activity of intravitreal VEGF trap.

Br J Ophthalmology 2008; 92 (5): 667-668

Stewart MW

Clinical and differential utility of VEGF inhibitors in wet age-related macular degeneration: focus on aflibercept.

Clin Ophthalmology 2012; 6: 1175-1186

Sulkes DJ, Ip MS, Bauman CR, et al.

Spontaneous resolution of vitreomacular traction documented by optical coherence tomography.

Arch Ophthalmology. 2000; 118: 286-287

Swanson EA, Izatt JA, Hee MR, et al.

In-vivo retinal imaging by optical coherence tomography.

Optics Letters 1993; 18:1864–1866

Toth CA, Narayan DG, Boppart SA, et al.

A comparison of retinal morphology viewed by OCT and by light microscopy.

Arch Ophthalmology 1997; 115: 1425–1428

Uchino E, Uemura A, Ohba N

Initial stages of posterior vitreous detachment in healthy eyes of older persons evaluated by optical coherence tomography.

Arch Ophthalmology 2001; 119: 1475-1479

Vingerling JR, Hofman A, Grobbee DE, et al.

Age-related macular degeneration and smoking.

Arch Ophthalmology 1996; 114: 1193-1196

Vinorez SA, Campochiaro PA, Conway BP

Ultrastructural and electron-immunocytochemical characterization of cells in epiretinal membranes.

Invest Ophthalmology Vis Sci. 1990; 31: 14-28

Witkin AJ, Patron ME, Castro LC, et al.

Anatomic and visual outcomes of vitrectomy for vitreomacular traction syndrome.

Ophthalm Surg Lasers Imaging. 2010; 41: 425-431

Wolf-Schnurrbusch et al.

Macular Thickness Measurements in Healthy Eyes Using Six Different Optical Coherence Tomography Instruments.

Invest Ophthalmology Vis Sci 2009; Vol 50, No 7: 3432-3437

Wojtkowski M, Bajraszewski T, Gorczynska I et al.

Ophthalmic imaging by spectral optical coherence tomography.

Am J Ophthalmology 2004; 138: 412-419

Wojtkowski M, Leitgeb R, Kowalczyk A, et al.

In vivo human retinal imaging by Fourier domain optical coherence tomography.

J Biomed Opt 2002; 7: 457–463

Wojtkowski M, Srinivasan V, Fujimoto JG, et al.

Three-dimensional retinal imaging with high-speed ultrahigh-resolution optical coherence tomography.

Ophthalmology 2005; 112: 1734–1746

Yaqoob Z, Wu J, Yang Ch

California Institute of Technology, Pasadena, CA,
USA

BioTechniques 2005, Vol. 39, No. 6: S6–S13

Yamada N, Kishi S

Tomographic features and surgical outcomes of
vitreomacular traction syndrome.

Am J Ophthalmology. 2005; 139: 112-117

Yamaike N, Tsjikawa A, Ota M, et al.

Three-dimensional imaging of cystoids macular
edema in retinal vein occlusion.

Ophthalmology 2008; 115: 355-362

Yanoff M, Duker J,S

Ophthalmology 3rd ed.

Basic and science

Elsevier, copyright © 2008; Section 6

Zawadzki RJ, Jones SM, Olivier SS, et al.

Adaptive-optics optical coherence tomography for high-resolution and high-speed 3D retinal in vivo imaging.

Opt Express 2005, 13: 8532-8546

7. Deutsche Zusammenfassung

Die Makula stellt das Zentrum des hinteren Pols im Auge dar und ist mit ihrer hohen Ortsauflösung wichtig für Fähigkeiten wie Lesen, Schreiben, Fahren oder Computerarbeit. Das Makulaödem (MÖ) ist die häufigste Pathologie im Bereich der Makula und resultiert in einer eingeschränkten Sehschärfe. Erkrankungen wie das diabetische Makulaödem (DMÖ), die altersbedingte Makuladegeneration (ARMD), retinale Gefäßverschlüsse und Veränderungen im Bereich der vitreoretinalen Schichtgrenzen stellen die häufigsten Gründe für ein MÖ dar. Durch Entwicklungen in der Pharmakotherapie können nun effektive Behandlungsmöglichkeiten für einige Makula-Erkrankungen bereitgestellt werden. Das MÖ geht mit morphologischen Auffälligkeiten im prä-, intra- und subretinalen Raum einher. Es wird zudem von Veränderungen im retinalen Pigmentepithel und der Choriokapillaris begleitet.

Bisherige technologische Fortschritte in der Optischen Kohärenz Tomographie (OCT) resultierten in hochauflösenden Bildern der Makula und erlauben die Darstellung morphologischer Veränderungen. Das Spectralis-OCT arbeitet mit einer Scangeschwindigkeit von 40.000 A-Scans pro

Sekunde bei einer axialen Auflösung von $7\mu\text{m}$ optisch bzw. $3,9\mu\text{m}$ digital. Es stellt somit ein effektives Hilfsmittel für die Detektion, Bewertung und Verlaufsbeurteilung von zentralen Retinadickenmessungen (CRT) und morphologischen Befunden in der Makula.

Es ist bekannt, dass trotz der Verbesserung der OCT-Techniken, Messungen im Bereich der Makula und deren Interpretation durch verschiedene Faktoren beeinflusst und somit variieren können. Zu den Störgrößen gehören z.B. Geräte verschiedener Hersteller, die Qualität der aufgenommenen Bilder, die Erfahrung des Befunders und nicht zuletzt die Komplexität der Befunde.

Unsere Ziele waren daher die Analyse der Übereinstimmung (intraobserver und interobserver) eines Allgemein-Augenarztes und eines erfahrenen Untersucher (Netzhaut-Spezialist) bei der Auswertung verschiedener Makulaveränderungen. Die Untersuchung umfasste die Messung der CRT und die Identifikation morphologischer Veränderungen in 500 Augen von 500 Patienten. Von der Gesamtzahl entfielen je 100 Augen auf fünf verschiedene Erkrankungen (altersbedingte Makuladegeneration, diabetisches Makulaödem, Venenastverschluss, Zentralvenenverschluss und epiretinale Membran).

Der Vergleich der ersten und zweiten CRT-Messung durch den Allgemein-Augenarztes (Intraobserver-Übereinstimmung) war statistisch nicht signifikant. Deshalb lässt sich sagen, dass die CRT-Messungen des Allgemein- Augenarztes in den beiden aufeinander folgenden Serien zeigten keine wesentlichen Unterschiede sowohl in Bezug auf die gesamten Augen als auch in Bezug auf die einzelnen Erkrankungsbilder.

Bei der ersten Interobserver-Analyse zeigten die CRT-Messungen bei Augen mit ARMD ($P=0,81$) und CRVO ($P=0,35$) eine gute Übereinstimmung. Bei Augen mit DME ($P<0,02$), BRVO ($P<0,04$) und ERM ($P<0,0007$) zeigte der Vergleich mit den CRT-Messungen eine unzureichende Übereinstimmung.

Die zweite Interobserver-Analyse für CRT-Messungen zeigte eine generelle Verbesserung des Allgemein-Augenarztes. Bei drei Pathologien, ARMD ($P=0,36$), CRVO ($P=0,55$) und DME ($P=0,08$) zeigte der Vergleich keine statistische Signifikanz. Der Vergleich von BRVO ($P<0,03$) und ERM ($P<0,02$) deckte eine statistische Signifikanz zwischen den Messungen der Befunder auf.

Bei der Auswertung vorgegebener morphologische Befunden konnte die höchste Übereinstimmung zwischen den Befundern bei der Identifikation von

Veränderungen innerhalb der Netzhautschichten wie z.B. MH, LMH, PSM, Vertikalisierung und Spaltung der Retina beobachtet werden. Die höchste Übereinstimmung war mit 78.4% bei der Diagnose des MH zu finden. Interessanterweise fand sich mit 38,6% die geringste Übereinstimmung bei ERM im präretinalen Raum, gefolgt von subretinalen Veränderungen im Bereich der ELM und der IS/OS- Schicht mit 43.6% bzw. 48.2%.

Insgesamt konnten wir feststellen, dass Intra- und Interobserverunterschiede bei unterschiedlichen Makulopathologien bzw. deren Auswertung anhand von Bildbefunden des Spectralis-OCT bestehen. Eine Trainingszeit von drei Monaten resultierte in einer teilweise besseren Interpretationsfähigkeit Makula-Morphologien durch den Allgemein-Augenarzt.

Basierend auf unseren Untersuchungsergebnissen muss jedoch davon ausgegangen werden, dass eine längere Trainingszeit mit intensiviertem Lernen (z.B. mittels interaktiven Möglichkeiten) notwendig ist, um eine zuverlässige Analyse von Spectralis-OCT-Bildern mit Makulaveränderungen durch den Allgemein-Augenarzt zu erreichen.

8. Acknowledgement

I want to express my sincere thanks to:

Prof. Dr. med. Faik Gelisken, Director of my Thesis, for his teaching, for his valuable suggestions, patience, interest and support throughout this Thesis.

Prof. Dr. med. K.U. Bartz-Schmidt, Medical Director and Chairman of the Department of Ophthalmology University of Tübingen, for giving me the opportunity to do my Fellowship and Doctorate program in Germany, for his teaching, for his valuable suggestions, interest and support.

Dr. med. Martin Leitritz, for his valuable suggestions, for always having time, for his interest and support throughout this thesis.

Prof. Dr. med. Jesús Ancer Rodriguez, Rector of the Universidad Autónoma de Nuevo León (UANL), for giving me the opportunity to do my Fellowship and Doctorate program in Germany, for his valuable suggestions, interest and support.

Prof. Dr. med. Santos Guzmán López, Director of the Hospital Universitario, 'Dr. José Eleuterio González' Universidad Autónoma de Nuevo León (UANL), for giving me the opportunity to do my

Fellowship and Doctorate program in Germany, for his valuable suggestions, interest and support.

My Father, Professor Dr. med. Ezequiel Enrique Treviño Cavazos, for motivating me to start this Doctorate, for his love, for believing in me, for his teachings, interest, patience, unconditional support and help that I have always been given, which has shaped me for the better, and made me be a better person.

My Mother, for her love, unconditional support and understanding: she never stop motivating me to go a step further and never stop believing in me, for her prayers and her advice that made a difference in making me a good man.

To my wife and children, for believing in me, for supporting me, enduring, motivating, inspiring and not giving up. For their love, unconditional support and understanding, for the unity and love of our family gives us the strength to do great things. Her example also motivates me to be better.

To my parent's in-law for their love, unconditional support and understanding. Your help has always given me patience and motivation.

To my brothers, sisters, friends and all those people, teachers, colleagues, that with your help,

genuine support, comments, good wishes, understanding, encouragement and interest in one way or another involved in the initiation, development and / or completion of this Doctorate.

To God, for allowing things to happen, for the opportunity and direction, I have been given by him without his help and protection nothing is possible.

Thankyou

9. Curriculum vitae

Personal data

Name: Hugo Alejandro Treviño Rodriguez

Date of birth: 24.04.1981

Place of birth: Mainz, Germany

Marital status: Married

Education

Faculty of Medicine of the Universidad Autónoma de Nuevo León, México. Degree obtained Surgeon and Obstetrician in 2008.

Graduate in Ophthalmology from March 2008 to February 2011. Hospital “Dr. José E. González”, Monterrey, Nuevo León, México.

Experience

1.- Participant in the Investigation Program of Early Detection of diabetic retinopathy in the Department of Ophthalmology in the Hospital “José E. González” of the Universidad Autónoma de Nuevo León from August 2006 to July 2007. Monterrey, N.L, México.

2.- Certificate in the investigation Program of LOCS III a lens opacity classification system in the

Department of Ophthalmology in the Hospital “José E. González” of the Universidad Autónoma de Nuevo León from October 2008 to July 2010. Monterrey, N.L, México.

3.- Certificate in the investigation Program of DARC-VIEW 2 in the Department of Ophthalmology in the Hospital “José E. González” of the Universidad Autónoma de Nuevo León from October 2008 to February 2011. Monterrey, N.L, México.

4.- Collaborator on the thesis Macular Surgery in the Department of Ophthalmology in the Hospital “José E. González” of the Universidad Autónoma de Nuevo León from October 2008 to February 2011. Monterrey, N.L, México.

5.- Thesis for the degree of specialty in Ophthalmology: "Use of perfluorocarbons in Macular Hole Surgery." In February 2011. Monterrey, Nuevo León, México.

6.- Publication of Thesis „Idiopathic macular hole total thickness. Technique modified using heavy liquid". Posted in Medical University. 2012; 14:56-64 - vol.14 No. 55. Monterrey, Nuevo León, México.

7.- Doctor’s degree of the Medical Faculty of the Eberhard Karls University of Tübingen since April 2012 to date.